Technical University of Denmark

DTU

The height of the atmospheric boundary layer during unstable conditions

Gryning, Sven-Erik

Publication date:
2005

Document Version
Publisher's PDF, also known as Version of record

[Link back to DTU Orbit](#)

Citation (APA):
Gryning, S-E. (2005). The height of the atmospheric boundary layer during unstable conditions. Roskilde: Risø National Laboratory. (Denmark. Forskningscenter Risoe. Risoe-R; No. 1536(EN)).

DTU Library
Technical Information Center of Denmark

The height of the atmospheric boundary layer during unstable conditions

Sven-Erik Gryning

The height of the atmospheric boundary layer during unstable conditions

Sven-Erik Gryning

Tethersounding in Athens during the MEDCAPHOT-trace experiment, August 1994.

Denne afhandling er i forbindelse med de nedenfor anførte offentliggjorte afhandlinger af Det naturvidenskabelige Fakultet ved Københavns Universitet antaget til offentligt at forsvares for den naturvidenskabelige doktorgrad.

København den 3 November 2005

Flemming Nicolaisen
Kst. dekan

Batchvarova, E. and Gryning, S.E (1991). Applied Model for the Growth of the Daytime Mixed Layer. *Boundary-Layer Meteorol.,* **56**, 261-274.

Batchvarova, E. and Gryning, S.E. (1994). An Applied Model for the Height of the Daytime Mixed Layer and the Entrainment Zone. *Boundary-Layer Meteorol.*, **71**, 311-323.

Batchvarova, E. and Gryning, S.E. (1998). Wind Climatology, Atmospheric Turbulence and Internal Boundary-Layer Development in Athens during the MEDCAPHOT-Trace Experiment. *Atmos. Environ.,* **32**, 2055-2069.

Batchvarova, E., Cai, X., Gryning, S.E. and Steyn, D. (1999). Modelling Internal Boundary-Layer Development in a Region with a Complex Coastline. *Boundary-Layer Meteorol.*, **90**, 1-20.

Batchvarova, E., Gryning, S.E. and Hasager, C. B. (2001). Regional Fluxes of Momentum and Sensible Heat over a Sub-arctic Landscape during late Winter. *Boundary-Layer Meteorol.,* **99**, 489-507.

Beyrich, F. and Gryning, S.E. (1998). Estimation of the Entrainment Zone Depth in a Shallow Convective Boundary Layer from Sodar Data. *J. Appl. Meteorol.*, **37**, 255-268.

Gryning, S.E. and Batchvarova, E. (1990). Analytical Model for the Growth of the Coastal Internal Boundary Layer during Onshore Flow. *Quart. J. Roy. Meteorol. Soc.,* **116,** 187-203.

Gryning, S.E. and Batchvarova, E. (1994). Parametrization of the Depth of the Entrainment Zone above the Daytime Mixed Layer. *Quart. J. Roy. Meteorol. Soc.* **120,** 47-58.

Gryning, S.E. and Batchvarova, E. (1996). A Model for the Height of the Internal Boundary Layer over an Area with a Irregular Coastline. *Boundary-Layer Meteorol.* **78**, 405-413

Gryning, S.E. and Batchvarova, E. (1999). Regional Heat Flux over the NOPEX Area Estimated from the Evolution of the Mixed Layer. *Agric. For. Meteorol.,* **98-99**, 159-168.

Gryning, S.E. and Batchvarova, E. (2002). Marine Boundary Layer and Turbulent Fluxes over the Baltic Sea: Measurements and Modelling. *Boundary-Layer Meteorol.,* **103**, 29-47.

Gryning, S.E. and Batchvarova, E. (2003). Marine Atmospheric Boundary-Layer Height Estimated from NWP Model Output. *Int. J. Environ. Pollut.,* **20**, 147-153.

Nyrén, K. and Gryning, S.E. (1999). Nomogram for the Height of the Daytime Mixed Layer. *Boundary-Layer Meteorol.,* **91** , 307-322.

Abstract

The height of the convective atmospheric boundary layer, also called the mixed-layer, is one of the fundamental parameters that characterise the structure of the atmosphere near the ground. It has many theoretical and practical applications such as the prediction of air pollution concentrations, surface temperature and the scaling of turbulence. However, as pointed out by Builtjes (2001) in a review paper on Major Twentieth Century Milestones in Air Pollution Modelling and Its Application, the weakest point in meteorology data is still the determination of the height of the mixed-layer, the so-called mixing height.

A simple applied model for the height of the mixed-layer over homogeneous terrain is suggested in chapter 2. It is based on a parameterised budget for the turbulent kinetic energy. In the model basically three terms - the spin-up term and the production of mechanical and convective turbulent kinetic energy - control the growth of the mixed layer. The interplay between the three terms is related to the meteorological conditions and the height of the mixed layer. A stable layer, the so-called entrainment zone, which is confined between the mixed layer and the free air above, caps the mixed layer. A parameterisation of the depth of the entrainment zone is also suggested, and used to devise a combined model for the height of the mixed layer and the entrainment zone. Another important aspect of the mixed layer development exists in coastal areas where an internal boundary layer forms downwind from the coastline. A model for the growth of the internal boundary layer is developed in analogy with the model for mixed layer development over homogeneous terrain. The strength of this model is that it can operate on a very fine spatial resolution with minor computer resources.

Chapter 3 deals with the validation of the models. It is based in parts on data from the literature, and on own measurements. For the validation of the formation of the internal boundary layer over land, especially extensive data sets from the Lower Fraser Valley in Vancouver, Canada were useful. The performance of the model over water was examined on measurements of marine boundary layer developments over Christiansø in the Baltic Sea. The model is found to perform relative well for both small and large distance downwind from the shoreline. The validation covers a scale of 100 km.

In some practical applications meteorological data are taken as the output from operational Numerical Weather Prediction models. The mixing height is not a part of the model output but has to be determined from the available data. This aspect is dealt with in chapter 4. Methods that are used to determine the mixing height from the available data are examined and improvements suggested. Numerical Weather Prediction models have a rather coarse resolution. The issue of grid resolution and its effect on the estimated mixing height is discussed. It is found that the mixing height in the coastal zone is not resolved.

In chapter 5 a new method for determining the regional fluxes of momentum and sensible heat over chessboard type patchy landscapes is presented. It is based on inversion of the model for the growth of the mixed-layer in combination with a parameterized form of the blending height concept. An example from sub-arctic Lapland illustrates that the forest dominates both the aggregated (area averaged) momentum and heat fluxes, but in quite different ways.

Chapter 6 provides a description of present problems and gives an outlook for future research in the field.

Resume

Højden af det atmosfæriske grænselag er en af de parametre der anvendes til at karakterisere dets struktur. Den er af betydning ikke alene for teoretiske studier, men også for praktiske anvendelser i forbindelse med forudsigelse af luftforureningskoncentration, temperatur samt parameterisering af turbulensen i atmosfæren. Builtjes (2000) påpeger i et indlæg om de mest betydningsfulde fremskridt indenfor modellering af luftforurening i det 20ende århundrede, at af de parametre der anvendes til at beskrive strukturen af det atmosfæriske grænselag er højden den der er dårligst bestemt.

I kapitel 2 præsenteres en simpel model af højden af det atmosfæriske grænselag over fladt homogent terræn. Udgangspunktet er en parameterisering af den turbulente kinetiske energi. Modellen bygger på de tre vigtigste led i budgettet for den turbulente kinetiske energi - spin-up leddet samt produktionen af mekanisk og turbulent kinetisk energi. Modellen relaterer samspillet mellem de tre led til højden af grænselaget samt den atmosfæriske stabilitet. Grænselagets top udgøres af et stabilt lag, der kaldes indtrængningslaget eller entrainment laget, der befinder sig mellem det atmosfæriske grænselag og den frie atmosfære. En parameterisering af tykkelsen af entrainment laget foreslås, og anvendes til at konstruere en model der kombinerer højden af grænselaget og entrainmentzonen.

Kystområders meteorologi er helt forskellig fra det ovenstående idet der dannes et såkaldt internt grænselag ved overgangen mellem vand og land. En model for højden af det interne grænselag udvikles efter samme retningslinjer som modellen for homogent terræn. En af modellens fortrin er at beregninger af højden af det interne grænselag kan udføres på et finmasket net med relativt ringe computer ressourcer.

Efterprøvningen af de udviklede modeller er beskrevet i kapitel 3. Der er anvendt dels målinger fra litteraturen, dels egne målinger. Et sæt målinger fra Lower Fraser Valley, Vancouver, Canada af interne grænselag over land har været særdeles nyttige. Modellen er ligeledes afprøvet på målinger af det interne marine grænselag over Christiansø i Østersøen. Modellen viste sig at fungere udmærket både for små såvel som store afstande fra kysten.

I forbindelse med en række praktiske anvendelser bestemmes grænselagshøjden fra output fra numeriske modeller til vejrforudsigelse. Dette er emnet for kapitel 4. Højden af grænselaget er ikke blandt de variable der beregnes, men den kan bestemmes fra de beregnede data. Metoder til at bestemme grænselagets højde diskuteres og nogle forbedringer foreslås. Modellerne der anvendes til vejrforudsigelse opererer på et meget grovmasket net. Samspillet mellem størrelsen af nettet og de estimerede grænselagshøjder diskuteres. Der viser sig at være et alvorligt problem i kystområder.

I kapitel 5 præsenteres en nyudviklet metode til at bestemme aggregerede flukse af impuls (engelsk momentum) og varme over et område med vekslende overfladeforhold. Metoden er baseret på invertering af den før beskrevne model for væksten af grænselaget kombineret med en parameterisering af blending-højde begrebet. Kendes vindprofilen og væksten af grænselaget fra f. eks. radiosonderingerer det muligt at beregne den aggregerede impuls og varmefluks. Et eksempel på anvendelse af metoden i Finsk Lapland illustrerer at skov dominerer både de aggregerede fluks af impuls og varme, men på helt forskellige måder.

Kapitel 6 anfører en række udestående problemer omkring højden af det atmosfæriske grænselag og giver forslag til fremtidig forskning indenfor dette område.

4

The study consists of the present summary and the following papers. In the summary, the papers are referred to in italics.

Batchvarova, E. and Gryning, S.E (1991). Applied Model for the Growth of the Daytime Mixed Layer. *Boundary-Layer Meteorol.,* **56**, 261-274.

Batchvarova, E. and Gryning, S.E. (1994). An Applied Model for the Height of the Daytime Mixed Layer and the Entrainment Zone. *Boundary-Layer Meteorol.*, **71**, 311-323.

Batchvarova, E. and Gryning, S.E. (1998). Wind Climatology, Atmospheric Turbulence and Internal Boundary-Layer Development in Athens during the MEDCAPHOT-Trace Experiment. *Atmos. Environ.,* **32**, 2055-2069.

Batchvarova, E., Cai, X., Gryning, S.E. and Steyn, D. (1999). Modelling Internal Boundary-Layer Development in a Region with a Complex Coastline. *Boundary-Layer Meteorol.*, **90**, 1-20.

Batchvarova, E., Gryning, S.E. and Hasager, C. B. (2001). Regional Fluxes of Momentum and Sensible Heat over a Sub-arctic Landscape during late Winter. *Boundary-Layer Meteorol.,* **99**, 489-507.

Beyrich, F. and Gryning, S.E. (1998). Estimation of the Entrainment Zone Depth in a Shallow Convective Boundary Layer from Sodar Data. *J. Appl. Meteorol.*, **37**, 255-268.

Gryning, S.E. and Batchvarova, E. (1990). Analytical Model for the Growth of the Coastal Internal Boundary Layer during Onshore Flow. *Quart. J. Roy. Meteorol. Soc.,* **116,** 187-203.

Gryning, S.E. and Batchvarova, E. (1994). Parametrization of the Depth of the Entrainment Zone above the Daytime Mixed Layer. *Quart. J. Roy. Meteorol. Soc* **120,** 47-58.

Gryning, S.E. and Batchvarova, E. (1996). A Model for the Height of the Internal Boundary Layer over an Area with a Irregular Coastline. *Boundary-Layer Meteorol.* **78**, 405-413

Gryning, S.E. and Batchvarova, E. (1999). Regional Heat Flux over the NOPEX Area Estimated from the Evolution of the Mixed Layer. *Agric. For. Meteorol.,* **98-99**, 159-168.

Gryning, S.E. and Batchvarova, E. (2002). Marine Boundary Layer and Turbulent Fluxes over the Baltic Sea: Measurements and Modelling. *Boundary-Layer Meteorol.,* **103**, 29-47.

Gryning, S.E. and Batchvarova, E. (2003). Marine Atmospheric Boundary-Layer Height Estimated from NWP Model Output. *Int. J. Environ. Pollut.,* **20**, 147-153.

Nyrén, K. and Gryning, S.E. (1999). Nomogram for the Height of the Daytime Mixed Layer. *Boundary-Layer Meteorol.,* **91** , 307-322.

Contents

1 Introduction

The atmospheric boundary layer (ABL) is generally regarded as that part of the atmosphere where the influence of surface friction and heating and cooling is felt. The transfer of energy between the surface and the air is partly accomplished by turbulent eddies. Atmospheric turbulence in the ABL is produced primarily by wind shear and buoyancy. Wind shear is mainly generated by the surface friction, but there may also be wind shear due to baroclinity and meso-scale processes such as sea breezes. Heating of the ground is the main source of convective type turbulence. There is a continuous loss of turbulent kinetic energy into heat by dissipation; and in a stable stratified atmosphere cooling of the ground gives rise to negative buoyancy that also acts as a sink for turbulent kinetic energy. Other processes that influences the actual level of turbulence in the atmosphere are advection and the energy that is spend during convective conditions to facilitate the growth of the boundary layer by entrainment of the warm air from the free atmosphere into the cooler mixed-layer.

The height of the ABL, h, is one of the fundamental parameters that are used to characterise its structure (Gryning *et al.,* 1987). Depending on the dominant production mechanism of turbulence three basic ABL-regimes can be distinguished - the convective, the neutral and the stable boundary layer. The main source of turbulence in the convective boundary layer (CBL) stems from the heating by insolation causing a positive buoyancy at the surface. This can create thermal plumes which generate an intensive vertical exchange of energy and matter, and eventually all properties are well mixed over most of the CBL. The mixing is limited in its vertical extent by an inversion that marks the top of the CBL. The height of the CBL undergoes a typical daily variation, being small in the morning and reaching its maximum in the late afternoon. Furthermore, its height depends on the characteristics of the actual site. In Europe the height of the mixed-layer in the late afternoon is typically 1-2 km above the ground.
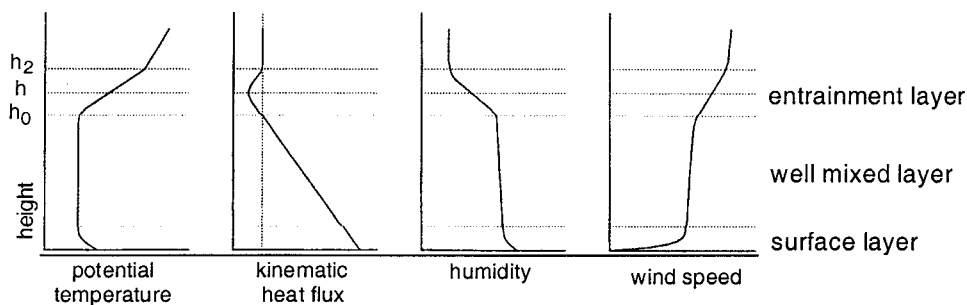
Figure 1.1. Schematic structure of the growing convective boundary layer (partly from Seibert et al. 1998). The surface in this case is more humid than the free atmosphere which is typical for vegetated areas.

The characteristic structure of the CBL in the growth phase is sketched in Fig. 1.1. Basically three structures can be distinguished:

1. The *surface layer* covers the lower 5-10% of the CBL. The turbulent fluxes of heat, moisture and momentum are assumed to be roughly constant with height in the surface layer. It is characterised by a pronounced wind shear in combination with a decrease of the potential temperature and specific humidity with height. The vertical profile of a number of meteorological variables such as wind speed and the variance

of vertical wind speed fluctuations are well described by the Monin-Obukhov similarity theory.

2. The *well mixed layer* takes up the major part of the CBL. Due to the intensive mixing in this layer, profiles of most meteorological variables are near constant with height. This is found to be a characteristic feature for the potential temperature but also a good approximation for specific humidity, as well as concentrations of trace gases and aerosols. The flow turns clockwise with increasing height (in the Northern hemisphere) and thus is in qualitative agreement with the Ekman profile.

3. The *entrainment zone* constitutes the transition between the mixed-layer and the stably stratified low-turbulence free atmosphere aloft. It is defined in a horizontally averaged sense. The layer is a result of the interaction of turbulent eddies and thermals at the top of the mixed-layer with the stratified free flow above. The penetration of energetic thermals into the stable layer aloft results in entrainment of warm and dry (in the absence of clouds) air from the free atmosphere above the entrainment zone. The entrainment zone comprises typically 20-40 % of the total depth of the CBL but can be even deeper than the mixed-layer especially in the morning when he mixed-layer is shallow and grows fast. Typical features of the entrainment zone are a positive gradient in the potential temperature, gradients (positive or negative) in the specific humidity and in aerosol and trace gas concentrations and, sometimes a strong vertical wind shear.

Figure 1.1 illustrates that two extreme definitions, h_2 and h_0 for mixing height are possible. From the numerous suggestions in the literature (see Stull, 1988; Garratt, 1990) it is clear that the practical determination of the mixing height, and even its definition, is not trivial. Seibert *et al.*, (2000) points out that the definitions often are made in the context of the models and data available to the authors. This also implies that there is no definitive or generally agreed way to measure a mixing height, the mixing-height meter does not exist. The most widespread definition, however, is the intermediate value h, where the gradient of the heat transfers reverses its sign. It is usually applied for scaling purposes and its is a height close to the thermodynamically CBL height definition in a zero-order jump model (i.e. a model where the entrainment layer is neglected, see Chapter 2). However, when using h for the mixing height one should be aware that turbulence extends beyond h.

A typical daily evolution of the CBL over land with continental climate on a clear sunny day (Seibert *et al.*, 1998) is described below.

1. Starting with the break up of the nocturnal inversion in the morning a shallow CBL is formed near the ground. It grows gradually until the nocturnal inversion has been completely eroded.

2. It is followed by a fairly rapid growth of the CBL through the slightly stable residual layer up to a level of the capping inversion from the previous day.

3. Thereafter the growth of the mixed layer is reduced as it penetrates into the stable stratified free atmosphere. At this stage large-scale vertical air motions (subsidence) that even might dominate over the penetration process and causing the mixed layer to decrease, can have a considerable influence on the evolution of the mixed-layer.

4. Eventually the thermally driven turbulence and vertical mixing decays which is followed by the formation of a shallow stable layer near the ground, which converts the CBL into the elevated residual layer for the following day.

In the absence of production of buoyant turbulence, the wind shear is the mechanism that creates turbulence. In a stably stratified atmosphere the negative buoyancy acts as a sink for the turbulent kinetic energy and a sensitive balance exists between production and destruction of turbulence. The general level of turbulence is low, other effects such as gravity waves, advection and subsidence may also influence the structure. Often the turbulence is not continuous but have an intermittent character. The stable boundary layer is not the topic for the present study, and therefore will not be dealt with further.

The classical way of describing the structure of the ABL is by use of similarity theories. It is assumed that the structure of the ABL depends on the height of the ABL, the height above ground z, and the turbulence parameters such as momentum and heat fluxes, that are combined into the Monin-Obukhov length scale L (Obukhov, 1946; Monin and Obukhov, 1954). The Monin-Obukhov length roughly equals to the height where production of mechanical and convective turbulence is equal. Depending on the distance from the ground and the atmospheric stability, certain scales may become irrelevant. Inspired by Nicholls and Readings (1979) the ABL was divided into domains each characterised by a set of scaling parameters (Holtslag and Nieuwstadt, 1986; Gryning *et al.*, 1987) where the basic dimensionless scaling parameters are taken as z/h and h/L, Fig. 1.2.
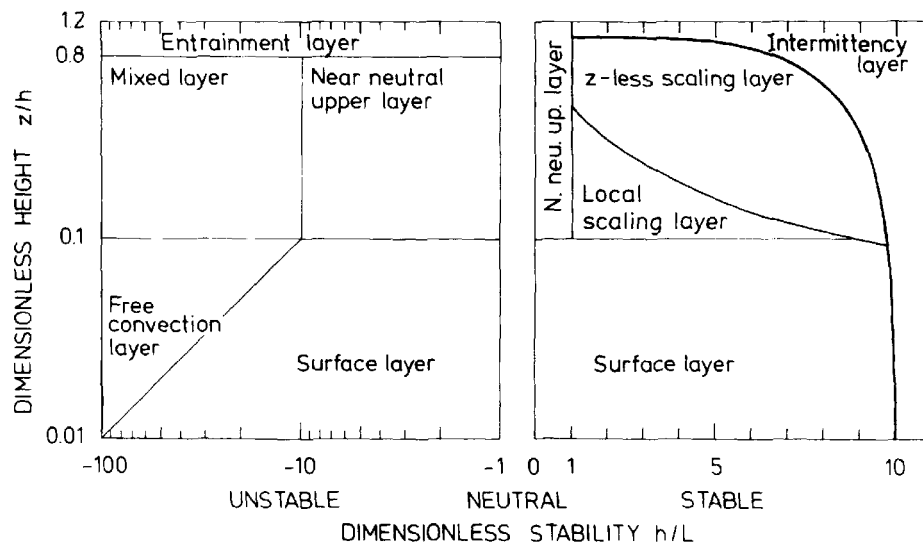
Figure 1.2. The scaling regimes of the atmospheric boundary layer. A detailed discussion can be found in Holtslag and Nieuwstadt (1986) and Gryning et al., (1987).

Historically the role of the h as scaling parameters in turbulence parameterisations was already pointed out by Deardorff (1970), but its role in the 70ties was mainly confined to be the upper limit of the volume that is available for the dispersion of pollutants released near the ground. It was considered a simple lid for use in Gaussian dispersion models or simple box models (Turner, 1970) that was assigned a constant value - usually 1000 m for atmospheric unstable conditions. Atmospheric stability was described by the famous Pasquill stability classification (Pasquill, 1974) that contrary to the Monin-Obukhov

11

length, can be determined from very simple, standard meteorological measurements. But already Klug (1968) and later Horst (1979) and Gryning *et al.* (1983) successfully applied the stability parameter z/L for determining plume spread from ground level sources at short distances where the influence of the mixing height is unimportant.

In the 80ties the Monin-Obukhov length gradually replaced the Pasquill classification for the description of the atmospheric stability and models appeared in which the vertical inhomogeneity of the turbulence characteristics within the ABL is considered both as function of z/L and of z/h (Gryning *et al.*, 1987). Parameterised profiles were used for quantities such as standard deviations if the turbulence wind velocity fluctuations and these, in turn, were related to the atmospheric dispersion process. The mixing height is not any longer just the parameter that limits the dispersion in the vertical direction. Now it is also taken into account in the parameterisation of the turbulence within the ABL.

The success of the Monin-Obukhov theory in atmospheric dispersion modelling was parallel to successful developments of schemes for the determination of the Monin-Obukhov length based on operational available meteorological parameters as demonstrated by *i. e.* Holtslag and van Ulden (1983). Today the Monin-Obukhov scaling length can also routinely be determined directly from measurements of turbulence. Good experience has been obtained with the use of ultrasonic anemometers for both measurements over long periods (years) and in harsh conditions such as during winter or in a marine atmosphere (Gryning *et al.*, 2001, *Gryning and Batchvarova, 2002*). The weakest point in the meteorological data is still the determination of the mixing height (Builtjes, 2001).

In recent years three-dimensional numerical models of the atmosphere has become an increasingly popular tool. From the model output regional patterns of the mixing height can be derived. *Batchvarova et al. (1999)* found good agreement between a comprehensive data sets on the mixing height in a coastal area and the mixing height that could be deduced from the meso-scale CSU-RAMS (The Colorado State University Regional Atmospheric Modelling System) model where the top of the mixing height was identified by a critical value in the turbulent kinetic energy. Also the output from Numerical Weather prediction (NWP) Models has been used to estimate the mixing height over extended areas. The NWP models do not, at least not until recently, calculate the turbulent kinetic energy in the routine mode, and hence the mixing height is determined from calculated wind and temperature profiles by use of the bulk Richardson-number methods (Seibert et al., 2000). The NWP models are generally represented on a much coarser grid than meso-scale models. Fay *et al.* (1997) report on a successful intercomparison with daytime measurements of the mixing height by a wind profiler/RASS system. Here the wind profile is determined from of a pulsed Doppler radar (around 1000 MHz) that is coupled to a radar acoustic sensing system (RASS) to determine the temperature profile (Engelbart, 1997). *Gryning and Batchvarova (2002)* discuss the mixing height over water in coastal areas deduced from NWP model simulations. It was found that when the grid resolution in the NWP model is of the same size as the distance to the coast the Richardson number method failed to predict mixing height over the water. It was also noticed that a commonly used version of the bulk Richardson number was dependent on the surface roughness *(Gryning and Batchvarova, 2003).*

When detailed output from meso-scale models or Numerical Weather Prediction Simulations is not readily available or available only on a grid too coarse to resolve the

mixing height in sufficient detail, then the modelling of the mixing height is almost entirely based on the so-called slab type models. Here the prognostic equation for the growth of the mixed layer is derived from the budget equations of temperature and turbulent kinetic energy (TKE). The equations proposed by various authors mainly differ in the terms that are neglected in the budget of the turbulent kinetic energy, and how the remaining terms are parameterised. The pioneering work goes back to Tennekes (1973) and Carson (1973) who only considered surface heating as the driving forces for the growth of the convective boundary layer. The effect of mechanical turbulence was discussed by Driedonks (1981), Yordanov and Batchvarova (1988) and *Gryning and Batchvarova (1990)*. The importance of the local change of turbulent kinetic energy due to entrainment of air with little TKE from the free air above the mixed layer, so-called spin-up was theoretically pointed out by Zilitinkevich (1975) and introduced in the modelling by *Gryning and Batchvarova (1990)*. Wind shear across the entrainment layer (Stull, 1976, Driedonks, 1981, Manins, 1982, Raynor and Watson, 1991); explicit parameterisations of the dissipation (Zeman and Tennekes, 1977) and complex relations taking into account energy losses in connection with gravity waves (Stull 1976), and the influence of moisture (Steyn 1990) have also been discussed. The studies by Driedonks (1981), Arya and Byun (1987) and *Batchvarova and Gryning (1991, 1994)* as well as sensitivity experiments reported by Beyrich (1995) have shown that the observed variability of the mixing height during daytime can in general be well described if surface heating and mechanical turbulence due to surface friction are taken into account, and with the entrainment heat flux parameterised in terms of the surface heat flux.

The objectives of this study is to investigate the dynamics and growth of the daytime mixed layer and present developments to produce a simple, slab-type model of the height, which is still sufficiently complex to retain the basic physical parameters controlling the growth of the mixed layer (Papers: *Batchvarova and Gryning (1991), Batchvarova and Gryning (1994), Beyrich and Gryning (1998), Gryning and Batchvarova (1994), Nyrén and Gryning (1999)*).

A closely related objective is to investigate the development of the internal boundary layers over an area with an abrupt change in surface conditions. The traditionally investigated example is the effect of a coastline. When cool air flows from the sea over land, the change in roughness and temperature creates a mixed-layer - so-called internal boundary layer. Because coastal areas are often urbanised due to the comfort for living created by the sea breeze and sometimes heavily industrialised because of the existence of a port, the internal boundary layer formation over this type of area is of major interest. However, other abrupt surface changes occur at field-forest borders and urban-rural and urban conglomerations in arid and semi arid areas. A major advantage of the simple slab model in this context is that it can be applied with a small grid size and therefore account for small scale variability. (Papers: *Batchvarova and Gryning (1998), Batchvarova et al. (1999), Gryning and Batchvarova (1990), Gryning and Batchvarova (1996), Gryning and Batchvarova (2002)*).

Finally some aspects of the derivation of the mixed-layer height from output from meso-scale and NWP models are discussed. (Papers: *Gryning and Batchvarova (2002), Gryning and Batchvarova (2003)*), and a new method for estimating aggregated (regional) momentum and heat fluxes over a patchy landscape is presented (*Gryning and Batchvarova, 1999; Batchvarova et al., 2001*). The method is based on inverting the model for the growth of the mixed-layer in combination with a parameterized form of the blending height concept.

2 Models

In this chapter the derivation of a simple slab-type model for the growth of the mixing height over homogeneous terrain, and a parameterisation of the depth of the entrainment zone above it will be outlined. By applying similar types of arguments a slab-type model for the growth of the internal boundary layer downwind from an abrupt change in surface conditions, as a sea-land transition, will be proposed. Details of the derivations are given in *Gryning and Batchvarova (1990), (1994)* and *Batchvarova and Gryning (1991) and (1994)*. The derivations are essentially based on the equation for heat conservation with no sources and sinks and the budget equation for the turbulent kinetic energy.

2.1 Slab model for the mixing height over homogeneous terrain

The derivation of the model for the growth of the mixed-layer is based on the zero-order scheme illustrated in Fig. 2.1. Following Deardorff (1979) a zero-order scheme does not attempt to predict the vertical thickness of the entrainment zone but it is idealised as being infinitesimally thin. A first order model takes into account that the temperature jump occurs over a significant vertical depth - as shown in Fig. 2.3.
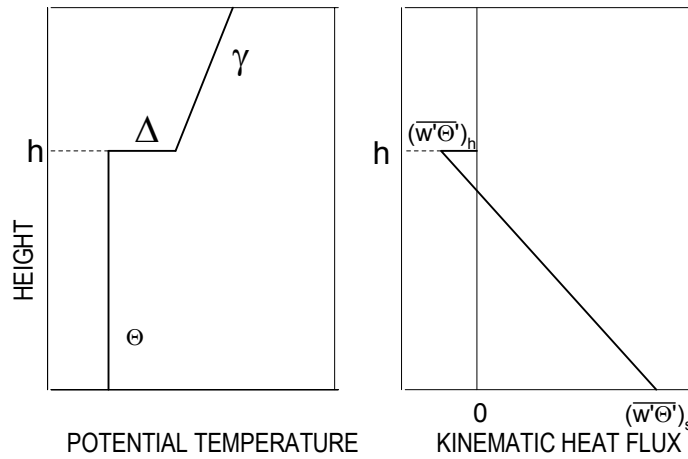
Figure 2.1. Illustration of potential temperature and sensible heat flux profiles in the zero-order model of the mixed layer.

Three of the governing equations comes from the heat conservation. For the downward vertical time-averaged heat flux at the top of the mixed layer $(\overline{\theta'w'})_h$ following Lilly (1968)

$$-(\overline{\theta'w'})_h = \Delta \frac{dh}{dt} \tag{2.1}$$

where Δ is the temperature jump at the top of the mixed-layer, t is time, θ is potential temperature and primes denote fluctuations from the mean. The inversion strength will tend to increase as the mixed layer entrains the warm air aloft, and decrease as the mixed layer is heated. Therefore

$$\frac{d\Delta}{dt} = \gamma \frac{dh}{dt} - \left(\frac{d\theta}{dt}\right)_{ml} \tag{2.2}$$

where γ is the potential temperature gradient above the mixed layer and the heating rate of the mixed layer, $(d\theta/dt)_{ml}$ can be expressed as:

$$\left(\frac{d\theta}{dt}\right)_{ml} = \frac{(\overline{\theta'w'})_s}{h} - \frac{(\overline{\theta'w'})_h}{h} \quad,$$
(2.3)

where $(\overline{\theta'w'})_s$ and $(\overline{\theta'w'})_h$ are the vertical kinematic heat flux at the surface and at the top of the mixed layer, respectively. However, one equation more is needed in order to derive an equation for the mixed layer height. The fourth equation is obtained from the parameterised budget for the TKE energy, discussed in the Appendix. With the spin-up term included, i.e. the term that represents spin-up of the turbulence from its small value in the free atmosphere to the state of the turbulence in the mixed layer (see also the Appendix), it reads:

$$-(\overline{\theta'w'})_h = A(\overline{\theta'w'})_s + \frac{Bu_*^3}{(g/T)h} - \frac{Cu_*^2}{(g/T)h}\frac{dh}{dt}$$
(A.9)

where g is acceleration due to gravity, T is temperature, g/T is the buoyancy parameter, u_* the friction velocity and the last term the co-called spin-up term. A, B and C are parameterisations constants, their values are discussed in the Appendix. The effect of humidity can be included by replacing $(\overline{\theta'w'})$ in Eq. (A.9) with $(\overline{\theta_v'w'})$ where θ_v is the virtual temperature. Driedonks (1982) found the effect of humidity on the height of the mixing layer to be less than 10%. Often the spin-up term is omitted, in which case the equation simplifies to read:

$$-(\overline{\theta'w'})_h = A(\overline{\theta'w'})_s + \frac{Bu_*^3}{(g/T)h} \quad .$$
(A.10)

By use of the Monin-Obukhov length:

$$L = -\frac{u_*^3}{\kappa(g/T)(\overline{\theta'w'})_s}$$
(2.4)

where κ is the von Karman constant, it is possible to derive the neutral and convective limits for the inversion strength Δ (*Batchvarova and Gryning, 1991*):

$$\Delta = \frac{1}{2}\gamma h + C^* h^{-1} \qquad \text{for} \quad L \to -\infty$$
(2.5)

$$\Delta = \frac{A}{1+2A}\gamma h + C^{**} h^{-(1+A)/A} \qquad \text{for} \quad L \to -0$$
(2.6)

where C^* and C^{**} are integration constants that can be determined from the initial conditions. *Gryning and Batchvarova (1990)* derived an analytical solution to Δ but it is unattractive for applied use. Neglecting the influence of the initial conditions an approximation to the analytical solution was suggested:

$$\Delta = \frac{Ah - B\kappa L}{(1+2A)h - 2B\kappa L}\gamma h \tag{2.7}$$

which has correct asymptotic limits for neutral and convective limits. It is illustrated in Fig. 2.2.
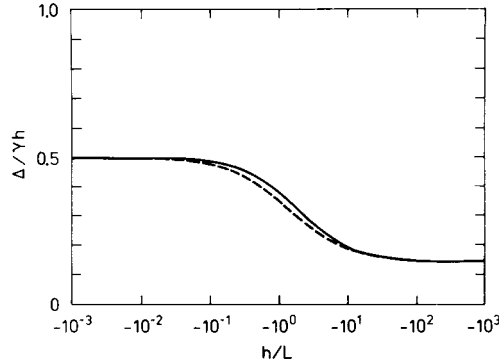

Figure 2.2. Dimensionless temperature difference across the inversion, $\Delta/\gamma h$, as function of the atmospheric stability. The solid line shows the analytical solution; the dashed line its approximation, Eq. (2.7).

Applying the expression for the parameterised heat flux at the top of the mixed layer that includes the spin-up term, and the approximation Eq. (2.7) for Δ the desired differential equation for h was derived (for details see *Gryning and Batchvarova (1990)* and *Batchvarova and Gryning (1991))*

$$\left\{\frac{h^2}{(1+2A)h - 2B\kappa L} + \frac{Cu_*^2}{\gamma(g/T)[(1+A)h - B\kappa L]}\right\}\left(\frac{dh}{dt} - w_s\right) = \frac{(\overline{\theta'w'})_s}{\gamma} \tag{2.8}$$

which is a practical, prognostic equation for h. *Gryning and Batchvarova (1990)* also suggested an analytical solution for h, which turns out to be implicit and consequently impractical. The effect of the mean vertical motion, w_s of the air at the top of the boundary layer owing to large-scale subsidence has been introduced in Eq. (2.8). It can be estimated when the horizontal divergence:

$$div_H = D^{-1}\int_D\left(\frac{\partial u}{\partial x} + \frac{\partial v}{\partial y}\right)dx\,dy \tag{2.9}$$

of the large-scale flow is known as function of height. Here D represents the surface area. For the special case of horizontal divergence constant with height, w_s can be expressed as

$$w_s = -(div_H)h \qquad . \tag{2.10}$$

A detailed description of the formal derivation is given in *Batchvarova and Gryning and (1994)*.

The horizontal divergence, div_H, can be estimated when wind measurements from a network of meteorological stations are available (Boers *et al.*, 1984). *Gryning and Batchvarova (1999)* devised a method based on the rate of warming caused by subsidence $\partial\theta(z)/\partial t$ of the free atmosphere above the mixing layer at height z

16

$$div_H = \left(\frac{\partial \theta(z)}{\partial t} \right) \Big/ \gamma \; z \qquad (2.11)$$

where $\gamma(z)$ is the gradient in the free atmosphere of the potential temperature at height z. Both $\partial \theta(z)/\partial t$ and $\gamma(z)$ can adequately be determined from successive radiosoundings.

The divergence of the wind field can locally be very different from the large scale value, resulting in a considerable change of mixed layer height that is not expected from large scale considerations. Local divergence can be caused by inhomogeneous terrain such as mountains or changes in surface properties, or associated with the evening transition of the boundary layer.

The growth of the mixed layer, omitting subsidence, basically is controlled by three terms that are related to the spin-up effect, and to the production of mechanical and convective turbulence. It is an important aspect of the model that the relative importance of the terms changes with the meteorological conditions and the height of the mixed layer. Comparing the spin-up term (second term of the left-hand-side of Eq. (2.8) with the contribution from mechanical and convective turbulence (first term of the left hand side of Eq. (2.8)) it can be see (*Gryning and Batchvarova, 1990*) that the contribution to the growth of the mixed layer from the spin-up term is the larger up to a mixed-layer height of about 50 meters. Below this height the growth is controlled mainly by the spin-up term, and above by the mechanical and convective turbulence. The dividing height increases when u_* becomes larger and γ becomes closer to zero. In the limit of $\gamma \to 0$ the growth of the mixed layer is controlled entirely by the spin-up term. In this case the present formulation is inappropriate because it disregards the effect of the Coriolis parameter and the decrease of momentum flux as function of height, which limits the growth of the mixed layer beyond the surface boundary layer.

In a similar way the contribution from mechanical and convective turbulence to the growth can be evaluated from the first term on the left-hand-side. The contribution from mechanical and convective turbulence is the same, *Gryning and Batchvarova (1990)*, when

$$(1 + 2A)h = -2B\kappa L \qquad (2.12)$$

which corresponds to $h = 1.4 \, |L|$, where mechanical turbulence is dominating the growth when h is smaller than $1.4 \, |L|$. Basically the spin-up terms dominate the growth of the mixed layer when it is shallow. Further growth makes the contribution from mechanical production of turbulence increasingly important until the mixed layer reaches a height of approximately to $1.4 \, |L|$, where the convective turbulence takes over the control of the growth process. Depending on the prevailing meteorological conditions, the importance of the three processes varies in their importance for the growth of the mixed layer.

It has correctly been pointed out by Luhar (1998) that *Gryning and Batchvarova (1990)* include only the spin-up effect on h and omits the effect of the spin-up term in the parameterisation of Δ. Luhar (1998) also points out that the model proposed by *Gryning and Batchvarova (1990)* neglects the convective contribution to the spin-up term which makes the model singular for $\gamma = 0$ under convective conditions where u_* becomes

negligible. Luhar (1998) adds the convective velocity, w_* to the formulation of the spin-up term, where *Gryning and Batchvarova (1990)* only consider the friction velocity. With these additions to the model formulation Luhar (1998) extends the *Gryning and Batchvarova (1990)* formulation for Δ with an additional term

$$\Delta = (\Delta)_{GB} + (\Delta)_{\gamma=0} \tag{2.13}$$

where $(\Delta)_{GB}$ is the formulation given in Eq. (2.7) by *Gryning and Batchvarova (1990)* and $(\Delta)_{\gamma=0}$ is an additional term that represent the effect on the spin-up term from the convective velocity. This term secures that the mixed layer height remains limited for $\gamma \to 0$ under very convective conditions. With the initial conditions $\Delta = 0$ at $h = h_{init}$ Luhar (1998) suggest

$$(\Delta)_{\gamma=0} = \frac{3\delta A}{(3+2A)}\left[-\frac{(h+\eta)^{2/3}}{h} + \frac{(h_{init}+\eta)^{\frac{2}{3}+\frac{1}{A}}}{h(h+\eta)^{1/A}} \right] \tag{2.14}$$

where $\delta = \left(\left(\overline{\theta'w'}\right)_s^2 (g/T)^{-1}\right)^{1/3}\left(C/A^{1/3} B^{2/3}\right)$ and $\eta = Bu_*^3\left(A(g/T)\left(\overline{\theta'w'}\right)_s\right)^{-1}$. Use of this expression in the derivation of the formulae for the height of the mixed layer result in a more physical but complicated expression that can easily be programmed and solved on a computer. However it has lost its physical transparency.

2.2 Parameterisation of the depth of the entrainment zone

In the above model the entrainment zone was taken as infinitesimal thin, which is a crude approximation. The thickness of the entrainment zone is typically 30% of the mixed layer, but it can reach a depth comparable to the mixed layer itself. It is characterised by a temperature gradient significantly stronger than that of the overlying stably stratified air, by a usually sharp reduction in moisture and aerosol content, and sometimes by a significant wind shear. The entrainment zone is a result of the interaction of turbulent eddies or thermals at the top of the mixed layer with the stably stratified air above. Overshooting of thermals causes entrainment of large parcels of free air into the mixed layer. The energy required to maintain entrainment is supplied by mixed layer turbulent kinetic energy, which is generated continuously by wind shear and convection, and its structure is therefore closely connected to the growth of the mixed layer.

Gryning and Batchvarova (1994) devised a parameterisation of the thickness of the entrainment zone, based on a so-called first order model (Deardorff, 1979), portrayed in Fig. 2.3. In analogy to the zero-order model, the turbulence is assumed to be sufficiently intense to maintain a uniform distribution of the potential temperature within the mixed layer up to height h_0. The air immediately above constitutes an entrainment zone of thickness Δh. Above the entrainment zone in the free atmosphere the air is also stable but is assumed free of turbulence and with generally less thermal stratification. The height h is introduced in such a way that the heat deficit is conserved and corresponds to the mixing height that can be derived from zero-order jump models such as *Gryning and Batchvarova (1990)*.
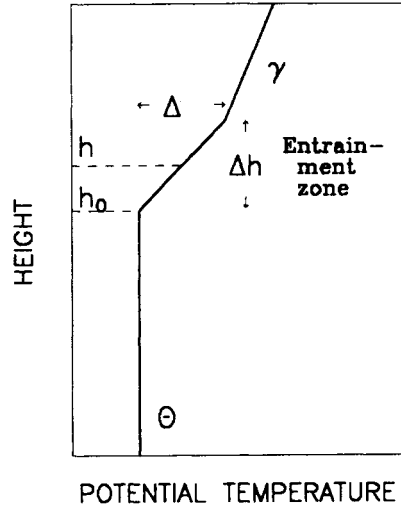
18

Figure 2.3. The idealised vertical profile of the potential temperature, a so-called first-order model that is used for the parameterisation of the entrainment zone.

By relating the rate of consumption of turbulent kinetic energy associated with the entrainment of free-atmosphere air in connection with the growth of the mixed layer to the vertical distance an air parcel penetrate into the stable stratified entrainment zone *Gryning and Batchvarova (1994)* found that the entrainment zone thickness $\Delta h / h$ can be parameterised as function of an entrainment Richardson number

$$Ri_E = \frac{(g/T)\, h\Delta}{(dh/dt)^2} \qquad .$$

(2.15)

The parameterisation can be written as

$$\frac{\Delta h}{h} \propto Ri_E^{-1/3}$$

(2.16)

where the constant of proportionality between $\Delta h/h$ and $Ri_E^{-1/3}$ has to be determined from measurements. Two data sets were used in this context, one based on water tank experiments (Deardorff *et al.,* 1980) and one based on experiments in the atmosphere reported by Boers and Eloranta (1986). From Fig. 2.4 it can be seen that the data orders rather nicely. The data sets from Boers and Eloranta (1986) and Deardorff *et al.,* (1980) supplement each other covering a range of Ri_E from 10^2 to 10^8 with overlap among the data sets around $Ri_E \approx 10^4$. The data of Deardorff *et al.,* (1980) suggests an asymptotic limit for $\Delta h/h$ of around 0.2. In Fig. 2.4 the solid line

$$\frac{\Delta h}{h} = \frac{3.3}{Ri_E^{1/3}} + 0.2$$

(2.17)

combines the asymptotic empirical limit for $\Delta h/h$ with the -1/3 power law of Ri_E, and constitute the suggested parameterisation for the depth of the entrainment zone. Emphasis in the fit is on measurements having large variability in Ri_E and with less focus on the group of points around $Ri_E \approx 10^4$.
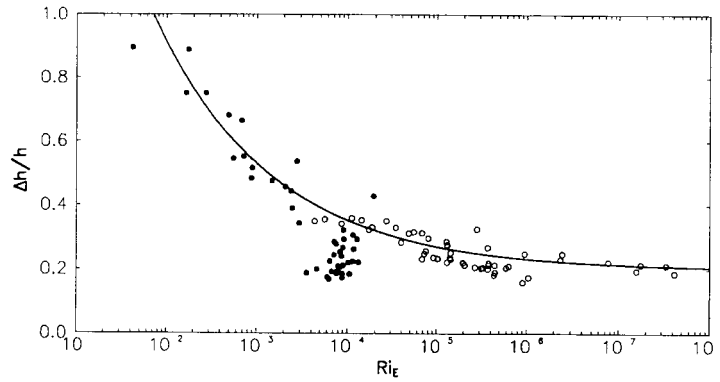
Figure 2.4. Normalised depth of the entrainment zone plotted as function of the entrainment Richardson number Ri_E. Open circle represent data from Deardorff et al. (1980) and filled circles data from Boers and Eloranta (1986) of which only clear sky conditions are considered. The solid line is the relationship suggested in Eq. (2.17).

2.3 Hybrid model for the height of the mixed layer and the entrainment zone

It is interesting to note, (*Batchvarova and Gryning, 1994*) that the zero-order model of the growth of the mixed-layer and the first-order parameterisation of the entrainment zone depth can be combined into a model for the growth of the mixed layer and the depth of the entrainment zone under near-neutral to unstable atmospheric conditions. The use of the combined model requires only those meteorological parameters that are needed in operational applications of ordinary slab type models; friction velocity, kinematic heat flux near the ground and potential temperature gradient in the free atmosphere above the entrainment zone. *Gryning and Batchvarova (1994)* give a thorough discussion of the formulation and application of the hybrid model.

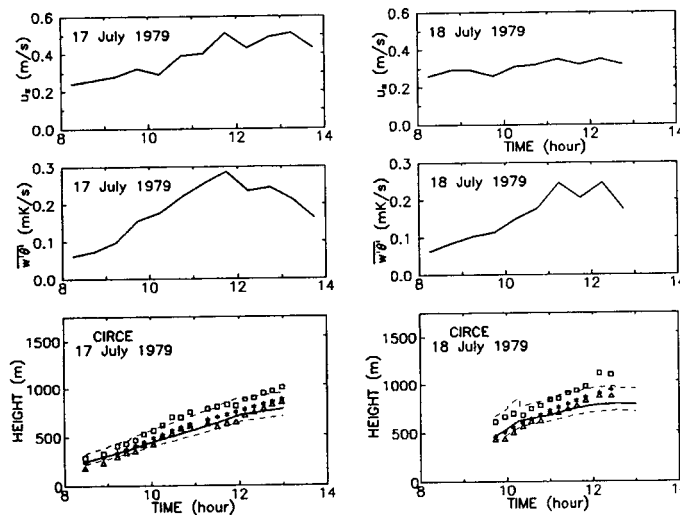*Figure 2.5. Example from the CIRCE experiment. The upper four panels illustrate the meteorological conditions. In the lower panels the lines show the simulation of the mixed layer height (solid line) and the predictions of the entrainment zone (dashed line) by the hybrid model. The symbols show measurements of the height of the mixed layer (*) and the upper (□) and lower (Δ) bounds of the entrainment zone.*

20

An application of the combined model is illustrated in Fig. 2.5 based on data from the Central Illinois Rainfall Chemistry Experiment, the so-called CIRCE experiment (Boers *et al.*, 1984; Boers and Eloranta, 1986). During this campaign the mixing height and structure of the entrainment zone was obtained by lidar. It can be seen in Fig. 2.5 that the CIRCE experiment represent fairly convective meteorological conditions with large vertical heat fluxes and small friction velocities.

It should be noted that the CIRCE data set contains information on large-scale horizontal divergence, which gives rise to large-scale vertical air motion. This is accounted for in the analysis presented in Fig. 2.5.

2.4 Slab model for the height of the internal boundary layer

Another important aspect of the formation of capping inversions exists when the air flows over an abrupt change in surface conditions. The traditional example is the internal boundary layer that forms downwind from a coastline at onshore flow. The abrupt change from water to land conditions produces an internal boundary layer, which begins at the shoreline and grows in depth with distance inland. Because the land surface generally is warmer than the sea the internal boundary layer is convective. Other changes as lake/land and land/forest also can create internal boundary layers. A model for the growth of an internal boundary layer downwind from a change in surface conditions was developed in analogy with the model for the mixed layer growth. Fig. 2.6 shows schematically the physical basis for the model.
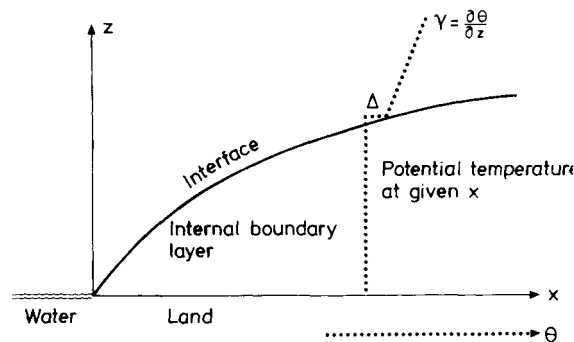

Figure 2.6. Schematic illustration of the physical system that forms the basis for the model of the development of the internal boundary layer.

Above the internal boundary layer, air is stably stratified with a potential temperature gradient independent of height and time. Inside the internal boundary layer, turbulence is assumed to be sufficient to maintain a uniform vertical distribution of the potential temperature. The finite inversion Δ, that caps the internal boundary layer, is assumed to be infinitesimally thin. The derivation of the prediction equation for the height of the internal boundary layer as function of downwind distance is achieved by inserting the Euler relation

$$\frac{dh}{dt} = \frac{\partial h}{\partial t} + u\frac{\partial h}{\partial x} + v\frac{\partial h}{\partial y}$$
(2.18)

of the material derivative dh/dt into the expression for the growth of the mixed layer, Eq. (2.8), which results in a 2-D equation for the height of the internal boundary layer

$$\left\{\left(\frac{h^2}{(1+2A)h-2B\kappa L}\right)+\frac{Cu_*^2}{\gamma(g/T)[(1+A)h-B\kappa L]}\right\}\left(\frac{\partial h}{\partial t}+u\frac{\partial h}{\partial x}+v\frac{\partial h}{\partial y}-w_s\right)=\frac{\overline{(\theta'w')}_s}{\gamma} \quad (2.19)$$

where u and v are the horizontal components of the mean wind speed in the mixed layer in the x- and y- directions – usually taken to be easterly and northerly directions, respectively. The model includes the effect of a complex coastline and allow for both spatial and temporal variations in the wind field and heat fluxes.

From Eq. (2.19) the development of the internal boundary layer in the 1-D case with negligible subsidence, and constant wind speed and heat flux can be investigated. In the limit of very convective conditions and omitting the spin-up term, the growth rate can be written as

$$\frac{u}{1+2A}h\frac{dh}{dx}=\frac{\overline{(\theta'w')}_s}{\gamma} \tag{2.20}$$

and with the boundary conditions $h=0$ for $x=0$ the boundary layer development downwind becomes parabolic

$$h=\sqrt{\frac{2(1+2A)\overline{(\theta'w')}_s x}{\gamma u}} \qquad . \tag{2.21}$$

In the limit of neutral boundary layers Eq. (2.19) can be written

$$u\left(\frac{h^2(g/T)}{2Bu_*^3}+\frac{C}{Bu_*\gamma}\right)\frac{dh}{dx}=\frac{1}{\gamma} \qquad . \tag{2.22}$$

Eq. (2.22) may be divided into two parts where the first on the left-hand-side represent the effect of the mechanically produced turbulence. With the usual boundary conditions it can be integrated to yield

$$h=\left(\frac{6Bu_*^3 x}{(g/T)\gamma u}\right)^{1/3} \qquad . \tag{2.23}$$

The second term on the left-hand-side represents the spin-up

$$\frac{dh}{dx}=\frac{Bu_*}{Cu} \tag{2.24}$$

which shows that when the internal boundary layer is shallow its growth is proportional to u_*. For $(B/C)=1.3$ Eq. (2.24) conforms with the theory of Miyake reported in Panofsky and Dutton (1984) for the growth of the internal boundary layer, and this value is recommended here. It was pointed out by Källstrand and Smedman (1997) that the value $(B/C)=0.3$ suggested by Driedonks (1982) actually refers to the growth of the equilibrium layer, the layer near the ground where the turbulence is in full equilibrium with the surface conditions, and not the growth of the internal boundary layer. The equilibrium layer constitutes roughly the lowest 10 per cent of the internal boundary layer.

It should be noted that the formulation of the spin-up term in *Gryning and Batchvarova (1990)* differs slightly from the one that is used here which follows *Batchvarova and*

Gryning (1991). The counterpart to Eq. (A.9) in *Gryning and Batchvarova (1990)* reads $-(\overline{\theta'w'})_h = A(\overline{\theta'w'})_s + Bu_*^3/((g/T)h) - Bu_*^2/(C(g/T)h)dh/dt$ and with this formulation Eq.(2.24) reads $dh/dx = Cu_*/u$. Therefore C in *Gryning and Batchvarova (1990)* equals B/C in the formulation used in *Batchvarova and Gryning (1991)* while the values of A and B remain the same.

By inserting the wind profile for neutral conditions into Eq. (2.24)

$$u(z) = \frac{u_*}{\kappa} \ln\left(\frac{z}{z_0}\right) \tag{2.25}$$

it integrates with the initial conditions $h = z_0$ for $x = 0$ to

$$\frac{x}{z_0}\frac{B\kappa}{C} = \frac{h}{z_0}\left[\ln\left(\frac{h}{z_0}\right) - 1\right] + 1 \tag{2.26}$$

which can be approximated by

$$h \propto x^{0.8} \tag{2.27}$$

as was already pointed out by Pasquill (1974) in an analogous study on the vertical dispersion of plumes from ground level sources. The approximation is illustrated in Fig. 2.7
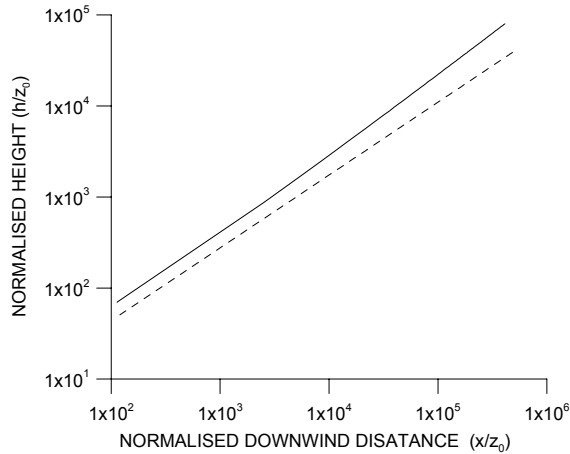
Figure 2.7. Normalised mixed-layer height as function of the normalised distance. The solid line is the relationship according to Eq. (2.26). The dashed line illustrates that h is near proportional to $x^{0.8}$, Eq. (2.27).

2.5 Model summary

The main model developments that has been presented in the foregoing chapters are:

A simple applied slab model for the height of the of the mixing-layer over homogeneous terrain:

$$\left\{\frac{h^2}{(1+2A)h - 2B\kappa L} + \frac{Cu_*^2}{\gamma(g/T)[(1+A)h - B\kappa L]}\right\}\left(\frac{dh}{dt} - w_s\right) = \frac{(\overline{\theta'w'})_s}{\gamma} \tag{2.8}$$

where w_s accounts for the vertical velocity of the air at the top of the internal boundary layer owing to large-scale subsidence. Generally w_s is difficult to estimate. A simple method to estimate w_s, based on the heating of the free atmosphere which can be estimated from successive radiosoundings, is proposed.

A parameterization of the entrainment zone thickness $\Delta h / h$ as function of an entrainment Richardson number

$$Ri_E = \frac{(g/T)\, h\, \Delta}{(dh/dt)^2} \qquad . \tag{2.15}$$

The parameterisation can be written as

$$\frac{\Delta h}{h} \propto Ri_E^{-1/3} \tag{2.16}$$

where the constant of proportionality between $\Delta h / h$ and $Ri_E^{-1/3}$ has to be determined from measurements. Based on two data-sets the empirical parameterization

$$\frac{\Delta h}{h} = \frac{3.3}{Ri_E^{1/3}} + 0.2 \tag{2.17}$$

was found to provides a good fit to the data.

A simple applied model for the height of the internal boundary layer that develops downwind from abrupt change in surface characteristics, typically a shoreline, as function of downwind distance. It is achieved by inserting the Euler relation

$$\frac{dh}{dt} = \frac{\partial h}{\partial t} + u\frac{\partial h}{\partial x} + v\frac{\partial h}{\partial y} \tag{2.18}$$

of the material derivative dh/dt into the expression for the growth of the mixed layer, Eq. (2.8). This results in a 2-D equation for the height of the internal boundary layer

$$\left\{ \frac{h^2}{(1+2A)h - 2B\kappa L} + \frac{Cu_*^2}{\gamma(g/T)[(1+A)h - B\kappa L]} \right\} \left(\frac{\partial h}{\partial t} + u\frac{\partial h}{\partial x} + v\frac{\partial h}{\partial y} - w_s \right) = \frac{(\overline{\theta' w'})_s}{\gamma} \tag{2.19}$$

where u and v are the horizontal components of the mean wind speed in the mixed layer in the x- and y- directions. When solved numerically the model can include the effect of inhomogeneous land use and a complex coastline

The rather complex interplay of the many processes that controls the general behaviour of the height of the mixed layer over flat terrain, as modelled by Eq. (2.8), is illustrated in the nomogram shown in Fig. 2.8 *(Nyrén and Gryning, 1999)*. The nomogram is specific for a given location. It takes into account information on the climatological air temperature, surface roughness and albedo. The nomogram is divided into 4 parts, the first represent curves of integrated heat flux (sensible plus latent) from dawn for a day without clouds as function of time of day on a monthly basis. The second part accounts for the effect of clouds and links the integrated flux to the impact of surface moisture on the height of the mixed layer for different wind speed conditions shown in the fourth table. The fourth frame also includes the effect of subsidence through the divergence of

the large-scale flow. Application of the nomogram is illustrated by following the arrowed line in Fig. 2.8.
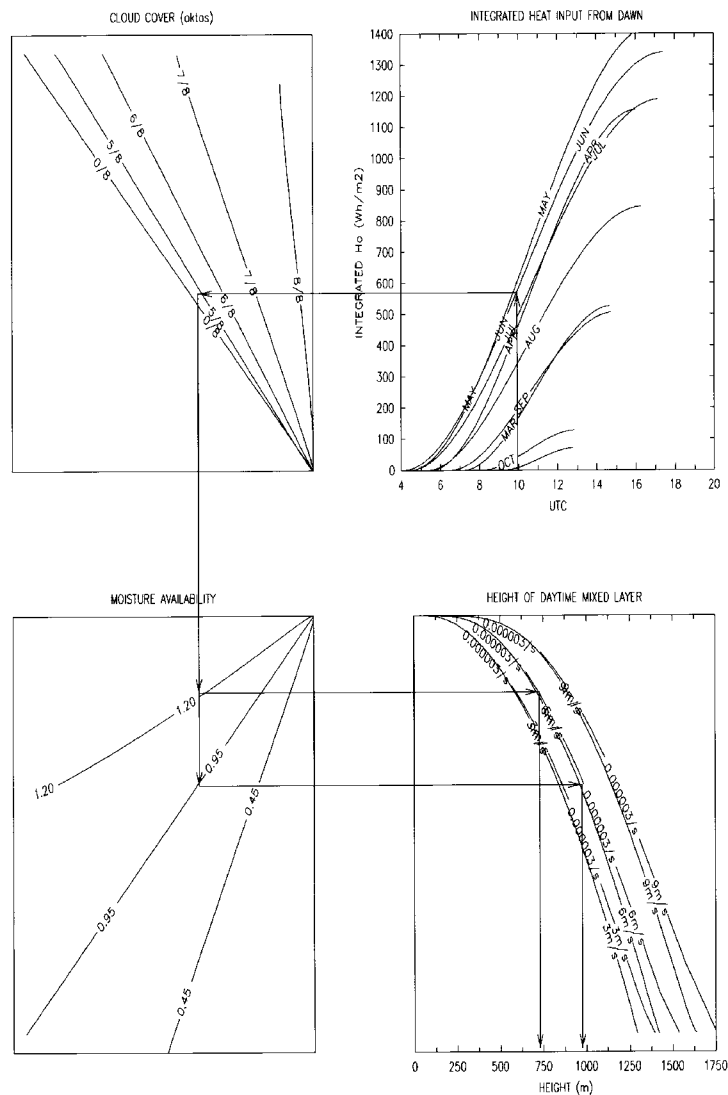

Figure 2.8 Nomogram for the height of the mixed layer at Marsta, Sweden. The arrowed line shows that at 1000= UTC in June for a 5 Octas cloud cover, a soil water availability of 0.95, and a wind speed of 6 ms^{-1}, the mixing height is 950 m.

Fig. 2.8 shows as an example the nomogram for Marsta, a location just north of Uppsala, Sweden. The arrowed line illustrates the estimation of the mixed layer height in June at 1000 UTC. For a 5 Octas cloud cover and a soil water availability of 0.95 (corresponding to grass land, Holtslag and van Ulden (1983)), a wind speed of 6 ms^{-1} at 10 meters height and no subsidence. The estimated height of the mixed layer corresponds to 950 m for grassland and reduced to 650 m for wet soil conditions (soil water availability of 1.2). It is clearly seen that, as expected, the cloud cover has a pronounced effect simply because it reduces the amount of solar radiation that reaches the ground. But it is interesting that also the soil moisture is a very important parameter for the growth of the mixed layer. In a dry area the mixed layer can get very high, but under similar conditions except for a wet surface the mixed layer growth is reduced.

A comparison of the nomograms for more southern locations reveals that the short winter days at Marsta results in low mixing heights as compared to the more southerly positions. During summer this behaviour is reversed (*Nyrén and Gryning, 1999*). The long days to the north results in comparable integrated heat fluxes at all three locations for similar surface conditions. This results in near similar mixing heights. However, difference in the soil moisture content among the sites might change this pattern.

It can be noted that for the development of the mixing height in sub-tropical and tropical conditions, the dependence on the water availability at the surface becomes very important. For arid or semi-arid areas, there is very limited water available for evaporation and the sensible heat flux becomes very large resulting in mixing heights of several kilometres. At high temperature over vegetated areas, the evaporation is consuming larger part of the available energy, and the latent heat expected to be larger than the sensible heat. Under these conditions the sensible heat and mixing height development is rather similar to European conditions under cloud free conditions. When the air is humid clouds form easily and energy becomes available from the phase transition from water vapours to cloud aerosols can create very large updrafts that lift the air high within the clouds. This effect is not included in the nomograms.

3 Validation

Considering the simplicity of the models, Eqs. (2.8) and (2.19), comparison with field measurements is essential. The first of several field campaigns was devoted to study the effect of the wind speed on the development of the mixing height over flat homogeneous terrain. This was done as part of Risø's contribution to an experimental campaign (devoted to study the wind field and atmospheric dispersion around a hill) in a very flat part of the Rhine valley about 40 km west of Cologne, Germany. The group from Risø used the opportunity to carry out additional measurements on development of the mixing height during conditions of moderate sensible heat fluxes and calm to moderate winds. The simulations of these measurements with the simple applied model demonstrated very clearly the importance of the wind speed (friction velocity) on the growth of the mixed-layer even at a moderate wind speed *(Batchvarova and Gryning 1991)*.

The model for the development of the internal boundary layer was evaluated in *Gryning and Batchvarova (1990)* against measurements from the literature. These experiments were on purpose carried out for a near constant wind speed and direction. They cover the Øresund region (Gryning, 1985), Nantikoke (Portelli, 1982; Kerman *et al.,* 1982) and Brookhaven (Stunder and SethuRaman, 1985).

Four cases of independent validations of the simple applied model illustrates that it is applicable under a large variety of meteorological conditions. Two of the experiments deal with the evolution of the internal boundary layer in coastal areas, one represents strong wind speed conditions and small heat fluxes; the other moderate wind speed with large heat fluxes over land. The third campaign represents the development of the mixed layer over flat terrain in southern Europe and the fourth mixed-layer development in the interior of the Antarctic plateau during summertime.

Källstrand and Smedman (1997) report results from an experimental study of the growth of the near-neutral coastal internal boundary layer. The campaign was carried out during two days in the fall of 1990 across the southern part of the Swedish coast. Measurements were carried out from an airplane flying along a line covering 20 km both upwind and

downwind of the coastline. The meteorological conditions represent relatively high wind velocities, about 7-10 ms^{-1}, from sea to land, small heat fluxes - of the order of 10 to 30 Wm^{-2} - and negligible temperature difference between the land and the sea. The measurements were compared with several empirical and similarity type expressions for the growth of the internal boundary layer, and a simplification of the *Gryning and Batchvarova (1990)* slab model in which the influence of heat flux was neglected. As many as 14 expressions for the growth of the internal boundary layer were tested. Källstrand and Smedman (1997) concluded that the majority of the models overestimate the height of the internal boundary layer. Some of the models give reasonable results for the first kilometres from the coast, but show large deviations from the measurements at larger distances. The model of *Gryning and Batchvarova (1990)* is the only formulation that agrees well with data for both small and larger distances from the coastline.

Melas and Kambezidis (1992) report results from the so-called ATHIBLEX campaign that was carried out in Athens, Greece during the summer of 1989 and 1990. The height of the internal boundary layer was determined from tethered soundings performed during sea-breeze conditions at the hill of Pnyx about 4 km inland. The wind speed over land was typically 4 ms^{-1}. The sensible heat flux was not measured directly but estimated from the substantial difference in surface temperature between the sea and land surface, typically 5 °C. During such conditions the heat flux in the centre of Athens (Pnyx hill) in August/September 1994 was measured to be 200-300 Wm^{-2} *(Batchvarova and Gryning, 1998)*. Melas and Kambezidis (1992) simulated the growth of the internal boundary layer with a total of 10 models. It was found that the slab models proposed by *Gryning and Batchvarova (1990)* gave the best result with a small bias (7 m) and a high correlation (0.80) with the observations. It should be noted that the model underpredicted the internal boundary layer height unless both the effect of mechanical and convective turbulence was taken into account. This is a very interesting result and shows that the large roughness of the town plays an important role with respect to growth of the internal boundary layer even at such large heat fluxes as in Athens.

Nardino *et al*. (2001) describes a micrometeorological campaign in the Po Valley, Italy, that was carried out during the fall of 1999 within the frame of the MAP programme (the Mesoscala Alpine Programme, http://www.map.ethz.ch). As part of the campaign, turbulence fluxes of heat and momentum were measured with sonic anemometers, and the mixed layer over the area was determined from radio soundings and SODAR measurements. The development of the height of the mixed layer was simulated for all clear days as well as a few partially covered days and compared to the measurements. Good agreement was found between measurements and their model simulations. The authors state, "the good agreement between computed and measured values demonstrates that the GB91 model is an optimum way to compute the time evolution of the mixed layer" (GB91 refers to *Batchvarova and Gryning (1991)*).

Argentini *et al.,* (2005) reports results from an experimental campaign carried out during the summer of 1999 and 2000 in the interior of the Antarctic plateau at Dome C. The mixing height development over the plateau was observed by a sodar and turbulence was measured by use of a sonic anemometer. The unstable mixed-layer reached a height of 250 to 400 metres at mid-day. The mixed-layer evolution was simulated by the model described in *Gryning and Batchvarova (1991 and 1994)*. The potential temperature profile and subsidence was not measured but use of typical values from an experiment in the Arctic gave qualitative agreement between measurements and model calculations.

However, these model comparisons for the development of the internal boundary layer in coastal areas were carried out under rather ideal conditions in terms of stationarity of the wind field. It was therefore a wish to extend the model validation to include the effect of a complex coastline and to allow for both spatially and temporal variations in the wind and heat fluxes.

3.1 Simulations of the height of the internal boundary layer over land

Data are available from a series of extensive investigations of increasing complexity and completeness in the Lower Fraser Valley in British Columbia, Canada, and participation in the so-called MEDCAPHOT-Trace campaign in Athens, Greece.

3.1.1 Experiments in the Lower Fraser Valley in 1976 and 1986

The Lower Fraser valley is characterized by a relatively flat floor surrounded by forested mountains to the north, east and south-east and a fairly complex coastline to the west and south, Fig. 3.1.
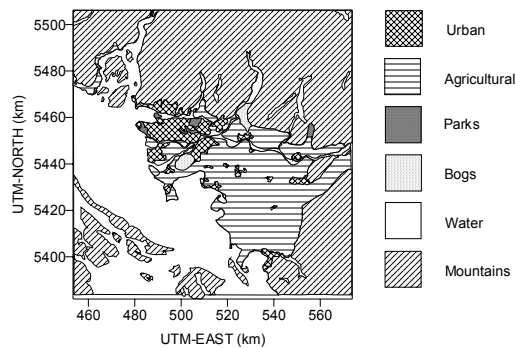

Figure 3.1. Map of the Lower Fraser Valley modelling domain and its land use.

The densely populated valley floor extends more than 60 km inland with a wide range of land use - urban areas including the City of Vancouver, agricultural and horticultural fields, parks and forests bogs and swamps, rivers and lakes.

Two rather similar experimental efforts were performed in 1976 and 1986 (Steyn and Oke, 1982; Cleugh and Oke, 1986). The data sets were collected at an observational site in the Sunset region south of Vancouver City, Figs. 3.1 and 3.4, situated approximately 10 km east of the coastline. The kinematic heat flux was measured by eddy correlation techniques.

Figure 3.2 shows an example of the simulated development of the internal boundary layer over the Vancouver area with Eq. (2.19). The calculations are started on July 31, 1986 at 06:30 LAT (local apparent time) with a weak southeasterly flow, which gradually turns towards the south. At 08:30 the flow is southerly resulting in a relatively long land fetch to the Sunset observational site. However, the flatness of the internal boundary layer height surface at that point indicates that its growth is controlled by the land surface and the effect of the water is not present. Throughout the following two hours the flow remains southerly. The pronounced structure that can be observed in the boundary layer at 10:30 LAT indicates that the effect of the water is now present over the whole modelling domain. At the observational site the boundary layer is very high, reaching 630 meters, and has a long land fetch. At 12:30 the height of the internal boundary layer at the Sunset site has diminished, the wind has now turned westerly

28

which results in a smaller land fetch, the wind speed is higher and the kinematic heat flux has increased. The wind direction remains westerly throughout the rest of the day.

Figure 3.3 shows the simulated and measured height of the internal boundary layer at the Sunset observational site for this experiment. In order to illustrate the effect of large scale divergence (subsidence) additional model simulations were performed neglecting subsidence. For this experiments which is carried out under low wind high pressure conditions the effect of subsidence is relatively important, lowering the height of the internal boundary layer by approximately 10 % in the afternoon. The effect in the morning is minor because the internal boundary layer is still shallow, which results in a small subsidence velocity.
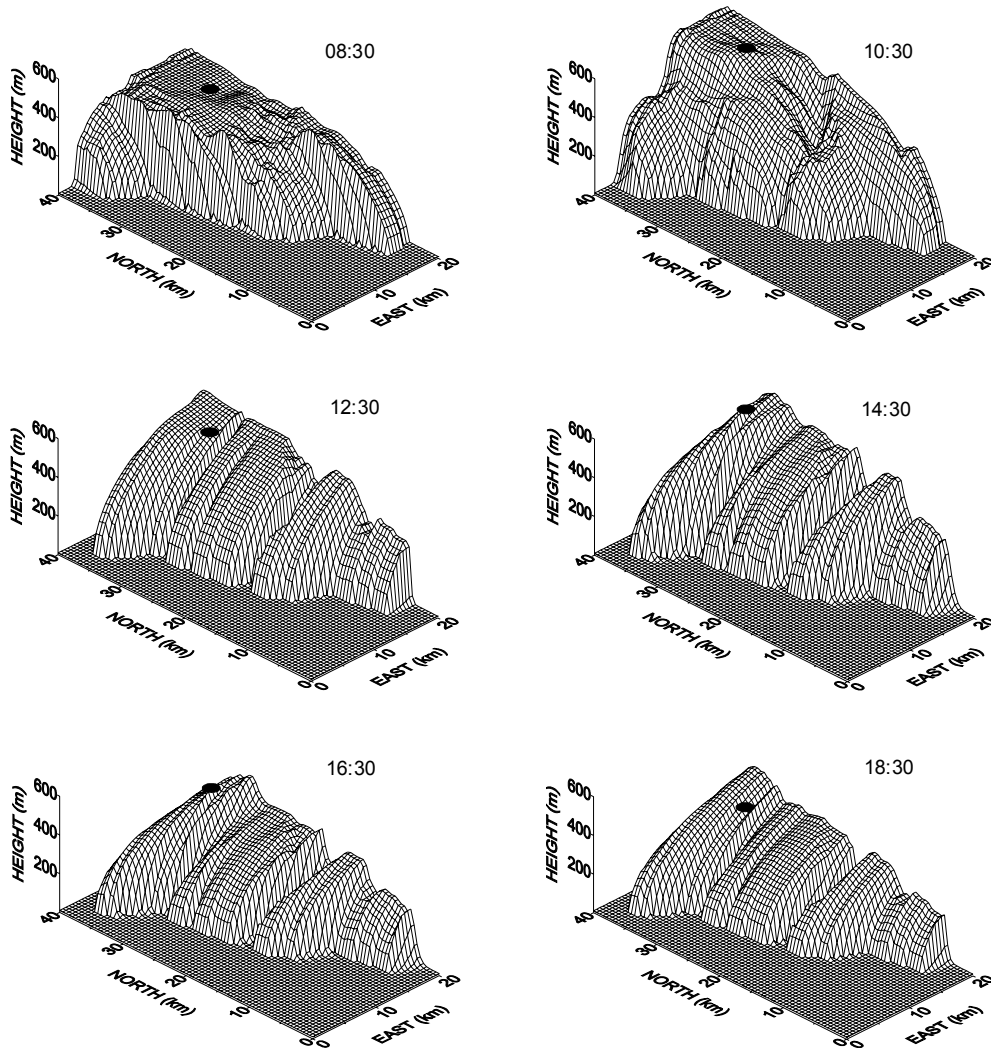

Figure 3.2. Simulated, Eq.(2.19), daily variation of the internal boundary layer over the Vancouver area on 31 July 1986. The bullet shows the location of the Sunset observational site (see Figs. 3.1 and 3.4) in the centre of the Vancouver.
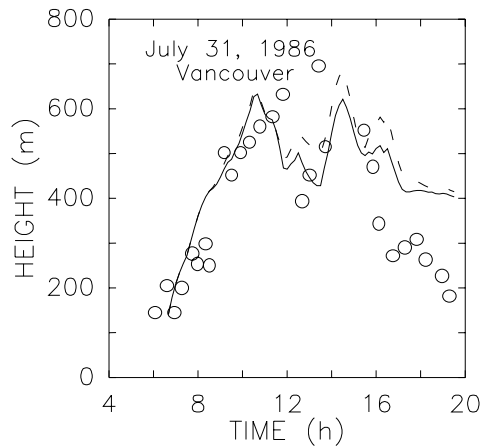
Figure 3.3. Mixed-layer height over the Sunset observational site (see Figs. 3.1 and 3.4) in central Vancouver. The simulation is performed with Eq. (2.19). Full line shows model results including subsidence, the dashed line excluding subsidence, and the bullets measurements.

The agreement between measurements and model results generally can be seen to be good. The good performance of the model is associated with the possibility of including the effects of changing wind direction and the irregular coastline which leads to varying land fetches, effects that are not easily accounted for in 1-D models. However, the simulations with Eq. (2.19) were based on measurements at only one location - which is a crude approach. A better approach will be to use measurements from a meteorological measuring network or calculated by meteorological models that reflect the inhomogeneous nature of the wind field over the area.

3.1.2 The PACIFIC-93 study

The above study initiated a collaboration with the University of British Columbia in Vancouver where we got access to data from a much more intensive field study, called PACIFIC-93, that was carried out in the Lower Fraser Valley in the summer of 1993 (Steyn *et al.,* 1997; Pottier *et al.,* 1994). Measurements of turbulent fluxes of heat and momentum were as in the previous study carried out at the Sunset observational site, Fig. 3.4.
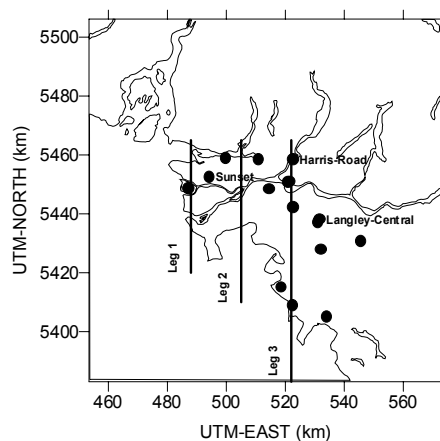

Figure 3.4. Map of the Lower Fraser Valley modelling domain showing the coastline (solid line), aircraft flight tracks (labelled 1, 2 and 3), and wind measuring sites (bullets).

30

The information on wind speed and direction was enhanced with information from a large number of routine meteorological stations. In the present study we used hourly data at 10 metres height from the 13 stations shown in Figure 3.4. Tethersonde measurements at Harris Road (Fig. 3.4) provided information on internal boundary layer height and the warming rate in the air above it. The PACIFIC-93 study furthermore provides a unique set of measurements on the spatial variability of the internal boundary layer in the region performed with a down-looking airborne lidar. Indicated on Fig. 3.4 are three legs from the afternoon flight that cover the transition from coastline to the valley floor. Internal boundary layer height can be diagnosed from these aircraft lidar images from the backscatter intensity, which distinguishes aerosol laden lower boundary layer air from the relatively cleaner upper boundary layer.

On 5 August, on the height of the study, the instruments were operated in a particularly intense effort. This day was characterised by warm, dry conditions as a stationary anticyclone dominated the regional weather. The spatial and temporal development of the internal boundary layer was simulated (*Batchvarova et al., 1999*) on a domain considerable larger than in the previous investigation, Fig. 3.1. The interpolated (*u)* and (*v*) wind field components in each grid point are derived by inverse distance squared interpolation to the measuring sites (weighted with $1/r^2$ where r is the distance from the actual grid point to the actual measuring sites) among the wind measurements at 13 land stations. The kinematic heat flux measured at the Sunset observational site was taken as a basis for the simulation with a correction applied in each grid point for the actual land use.

Figure 3.5 shows the simulated and measured height of the internal boundary layer at Harris Road. The agreement between measurements and model simulations is generally good but it is interesting to note that the model fails to simulate the lowering of the mixed layer in the afternoon. The lowering of the mixed layer might have many causes, one being local divergence in the wind field connected to the evening transition and the nearby mountains, effects that are not accounted for in the model.
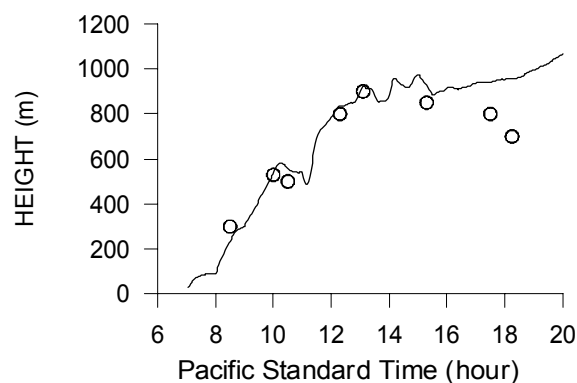

Figure 3.5. Temporal variation of the internal boundary-layer height simulated by the simple applied model, Eq. (2.19) and measurements (open circles) at Harris Road.

Observed and modelled spatial structure of the internal boundary layer height along two (leg 1 and 3) of the three flight legs is shown in Figure 3.6.
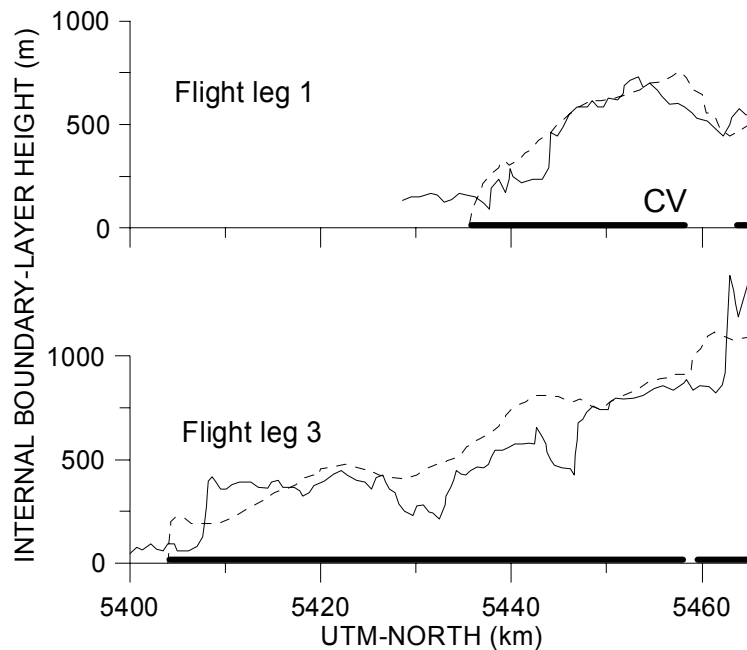
Figure 3.6. The spatial variation of the modelled, Eq. (2.19), internal boundary-layer height with the simple applied model (dashed line), and the measured height derived from aircraft data (solid line) along flight legs 1 and 3. The thick solid lines along the legs represent sections of land versus sea surface. CV shows the position of Central Vancouver.

In the southern part of flight leg 1 (Fig. 3.6) the internal boundary layer grows fast with a southerly wind blowing almost along the flight leg over the first 20 kilometres. Over Central Vancouver, the wind direction shifts slightly towards the west resulting in an overland fetch to the flight line of only 5 to 10 km. The internal boundary layer responds immediately to the shorter overland fetch by starting to decrease. This behaviour is clearly depicted in the measurements and reproduced in the model simulations. It nicely illustrates how sensitive the internal boundary layer height can be to a complex coastline where even small changes in the wind direction can result in pronounced variations of the overland fetch and consequently have large effects on the internal boundary layer. Flight leg 3 captures more than 50 kilometres over land. The southernmost 7 kilometres of the over land part of the flight line is parallel to the coast about 1 kilometre inland. The south-westerly wind in the area results in an overland fetch of about 1 to 2 kilometres to the flight line. Both the measured and modelled internal boundary layer is near constant along this part of the leg. After about 7 kilometres the coastline veers to the west away from the south-north flight line, resulting in renewed growth of the internal boundary layer in response to the increasing overland fetch. Twenty kilometres further to the north the internal boundary layer decreases. The map reveals that owing to the existence of two small bays the overland fetch is reduced and the internal boundary layer responds by decreasing. Further to the north the coastline veers of to the west, the land fetch becomes very long and the internal boundary layer starts to grow again.

Given the complexity of topography, coastline and land use in the Lower Fraser Valley region, the simple applied model generally perform rather well. It is clear that correct specification of spatially resolved surface sensible heat flux and wind field are crucial to the success of the model.

32

3.1.3 MEDCAPHOT-Trace campaign in Athens, Greece

Athens in Greece (as well as Los Angeles) is an outstanding example of an area with intense photochemical air pollution. In the late summer, sea-breeze circulations frequently form. Sea breeze conditions confine the air pollutants to a shallow internal boundary layer. Sea-breezes are characterised by rather weak winds - leading to high concentrations of air pollutants, and occur in conditions of strong insolation which favours the formation of photochemical pollution. The precise mechanism controlling the formation of the primary and secondary air pollutants and the interplay between the meteorological and chemical evolution is far from understood. The MEDCAPHOT-Trace (the MEDiterranean CAmpaign of PHOTochemical tracers - TRAnsport and Chemical Evolution) aimed to develop further understanding of the emissions, distributions and transport of ozone related trace gases in a typical Mediterranean coastal, densely urbanised area. The campaign was carried out in the Greater Athens Area, Greece, in August-September 1994, Fig. 3.7. Results from the MEDCAPHOT-trace campaign are published in a special issue of Atmospheric Environment (Ziomas, Gryning and Bornstein (editors), 1998). The resulting databank formed an important background for succeeding air pollution modelling efforts. As a curiosa it can be mentioned that the experience from MEDCAPHOT-Trace was used in connection with the assessment of the effect of ongoing (1997) and planned infrastructure improvements on the air pollution levels in the Greater Athens area when Athens was bidding for the Olympic game for 2004 (Moussiopoulos and Papagrigoriou, 1997).
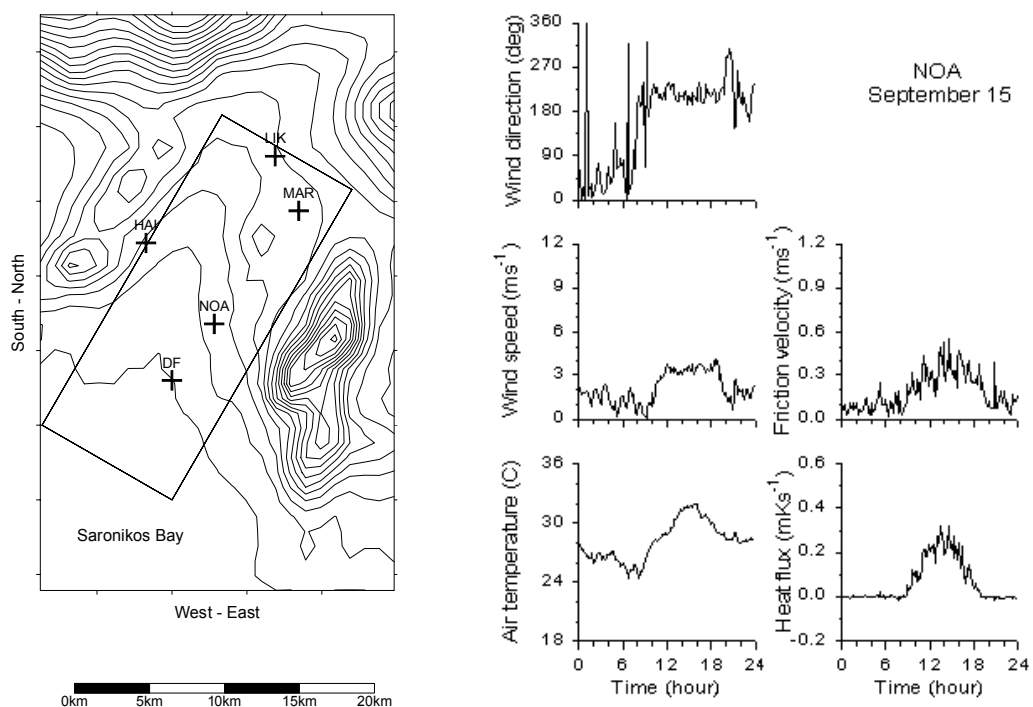
Figure 3.7. Left panel shows a map of the Greater Athens Area with the position of NOA - National Observatory of Athens - shown and additional sites with meteorological measurements. Contour lines are drawn in altitude steps of 50 m. The box shows the modelling domain. The right panels show measurements of fluxes and mean values carried out at NOA on September 15 (Batchvarova and Gryning, 1998). The shift in wind direction to SW at around 9-hour marks the arrival of the sea breeze. The measurements represent a typical air pollution episode.

Batchvarova and Gryning (1998) outlined the climatology of the wind and fluxes during the MEDCAPHOT-trace campaign. The considerable variation in the local meteorology over the Athens area is clearly seen. The campaign included the typical late-summer pattern with sequences of days with relative strong northerly winds, resulting in good ventilation of Athens and low air pollution levels, alternating with periods of sea breeze with low winds and shallow internal boundary layers, favourable of the formation of photochemical air pollution. The measurements show considerable variability in the meteorological conditions on the local scale. The internal boundary layer over the greater Athens was simulated with Eq. (2.19) for an air pollution episodes that occurred on 14-15 September 1997, Figs. 3.7 and 3.8. It is promising to see that even at such complicated conditions meteorological conditions as in Athens, comparison with measurements, although sparse, of the internal boundary layer height at NOA (National Observatory of Athens, located at Pnyx hill) about 4 km from the coastline shows good agreement with model results for two days with well developed sea breezes over Athens.
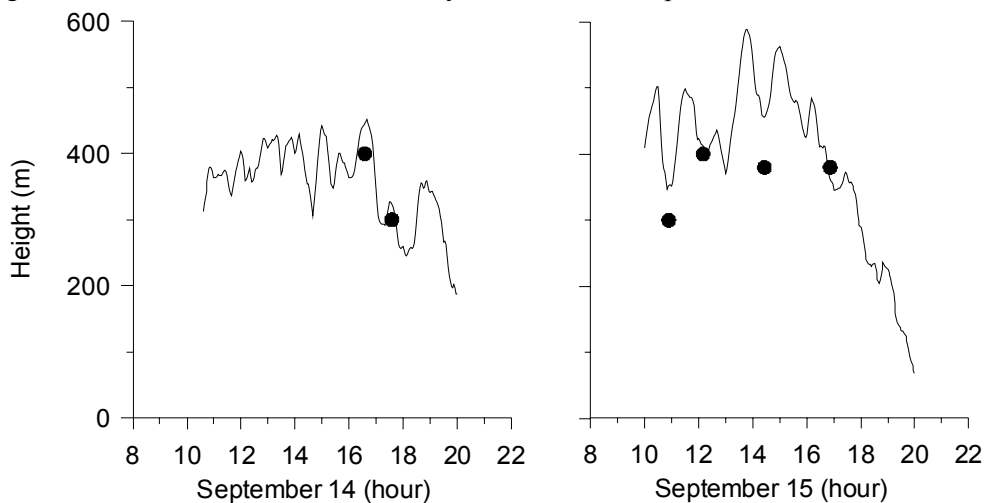

Figure 3.8. Simulated (Eq. (2.19) solid line) and measured (bullets) variation of the internal boundary layer over central Athens (NOA) during the air pollution episodes on 14 and 15 September 1994.

3.2 Simulation of the height of the marine atmospheric boundary layer

While the foregoing chapter dealt with the formation of the internal boundary layer over land, participation in PEP (Pilot study on Evaporation and Precipitation over the Baltic Sea) provided the opportunity to devote efforts on the atmospheric internal boundary layer that develops over the Baltic Sea. Data was obtained from a two-week measuring campaign carried out in the fall of 1998 (*Gryning and Batchvarova, 2002*). During the experiment the water was generally warmer than the air, which is a typical feature for the Baltic Sea during the late summer, autumn and early winter. This results in a generally positive sensible heat flux to the atmosphere, and the generation of a convectively driven boundary layer over the water.

The measuring activities were concentrated at a cluster of small islands in the Baltic Sea known as Christiansø, marked with a cross on Fig. 3.9. For south-westerly winds (sector 190° to 270°) Christiansø lies about 20 km downwind of Bornholm. For northerly winds (sector 270° to 45°) the water fetch to the Swedish coast is about 100 km.
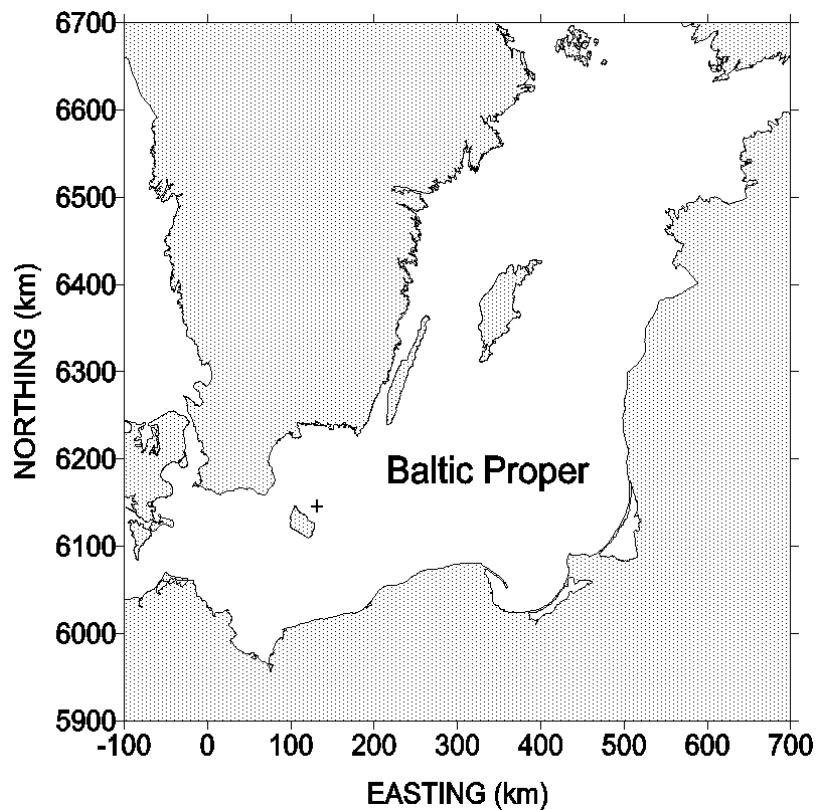
Figure 3.9. Map of the Baltic Proper with land surfaces and islands dotted. A cross shows the location of Christiansø east of Bornholm. The figure shows the domain where the simulations with the simple slab model, Eq. (2.19), were performed. The coordinate system refers to UTM34.

Measurements of atmospheric turbulent fluxes of sensible and latent heat and momentum were carried out on a small granite island with a large open sector to the sea. During an intensive observation period from 24 October to 5 November 1998 the depth of the boundary layer over Christiansø was estimated from frequently performed radiosoundings.

For this experiment we additionally have output from simulations with the numerical weather prediction model HIRLAM, described in chapter 4.

The height of the boundary layer was simulated for the period 26 October to 2 November 1998. The period from 26 October until midday 1 November 1998 is characterised by winds about 12 m s^{-1} from southwest to west. In this sector Christiansø is downwind of Bornholm with a water fetch of about 20 km. Following a wind direction shift on 1 November 1998 to northwest and north, the wind speed decreased to about 4 m s^{-1}. Then Christiansø is not downwind of Bornholm and the over water fetch from the Swedish coast is of about 100 km.

The simulation was based on the wind field from the HIRLAM model. Interpolated u (easterly direction) and v (northerly direction) wind field component at each grid point in the 2 km grid are derived for the whole model domain by inverse square interpolation between the wind predictions at the HIRLAM grid points. In the simulation the sensible heat flux and the friction velocity measured at Christiansø were used for the entire modelling domain. These parameters are expected to vary within the Baltic Proper. However the wind during the experimental campaign was between southwest and north,

corresponding to a water fetch to Christiansø from the nearest land of about 100 km or less. Under these conditions we assume the observations at Christiansø to be representative for the upwind sea-surface area.

The right panel in Fig. 3.10 shows the evolution of the simulated boundary-layer height over Christiansø, when the marine internal boundary layer starts to develop at the eastern coastline of Bornholm. The overall agreement is fairly good.
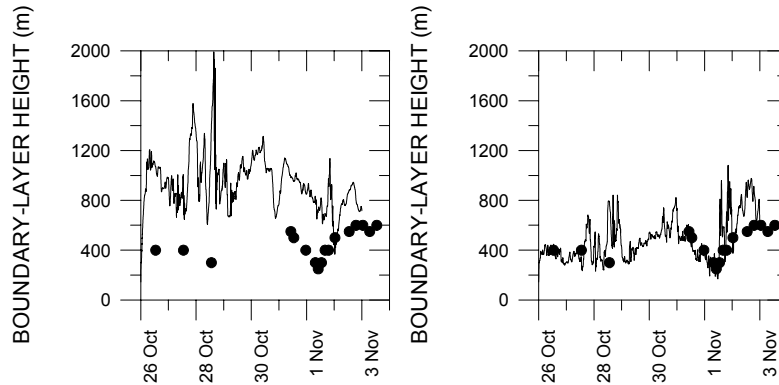

Figure 3.10. Simulations with the simple applied model, Eq. (2.19), of the evolution of the boundary-layer height over Christiansø during the extensive observation period. The solid line is the model simulation, the bullets show the observations of the boundary-layer height from the radiosoundings. On the left panel Bornholm is not accounted for but it is replaced by water. On the right panel the effect of Bornholm is accounted for in the simulation.

The left panel similarly shows the evolution of the boundary-layer height but without accounting for the effect of Bornholm. Bornholm is here replaced by water. It can be seen that for the period up till noon on November 1, the simulated boundary layer is markedly higher than the measured one. Thereafter the agreement becomes better. Inspecting the wind direction reveals that up till November 1 around noon, the wind is within the sector that includes Bornholm, and then the wind turns towards north and the air that reaches Christiansø has not passed over Bornholm on its way but comes from the Swedish coast.

The model simulation suggests that the distance to the island of Bornholm during the first period controls the boundary layer over Christiansø, and during the second period it is the distance to the Swedish coast.

3.3 Entrainment zone parameterisation

The above simulations were carried out with a zero-order model in which the entrainment zone is taken as infinitesimal thin. As found in *Gryning and Batchvarova (1994)* the thickness of the entrainment zone is typically 20-30% of the mixed layer, but can be comparable in thickness to the mixed layer itself.

Beyrich and Gryning (1998) used high-quality meteorological data collected within the SANA project (Schaller and Seiler, 1993) to test different parameterisations of the entrainment zone thickness suggested in the literature but with main focus on the *Gryning and Batchvarova (1994)* parameterisation. The field campaigns were carried out in 1991, 1993 and 1994 at a rural flat site in the south-eastern part of Germany about 50-km northeast of Leipzig. The experiments included high-resolution measurements (typically 20 s and 25 m resolution) with a non-commercial three-antenna monostatic

Doppler Sodar. It is possible to detect the entrainment zone in the records from the Sodar because the temperature gradient, wind shear, and associated thermal and mechanical turbulence in the entrainment zone results in enhanced backscatter of acoustic waves. Surface fluxes were measured by eddy-correlation techniques with an ultrasonic anemometer.

Based on the Sodar measurements the entrainment zone depth was estimated from 4 different methods that turned out to be quite consistent. The so-called percentile method uses the height difference between the 5%-10% and 90%-95% values of the cumulative frequency distribution of the instantaneous mixed-layer heights measured by the Sodar. Since this method seems to be the method that is most comparable to the definition of the entrainment zone by Deardorff *et al.* (1980) further discussions will be based on these estimates. Figure 3.11 shows $\Delta h/h$ against the entrainment Richardson number

$$Ri_E = \frac{(g/T)h\,\Delta}{(dh/dt)^2} \tag{2.12}$$

suggested by *Gryning and Batchvarova (1994)*, where the single data on the entertainment zone thickness are grouped according to their Ri_E values. The main part of the data falls within the range of the parameterisation, except for those that corresponds to large Ri_E values. This suggests that the asymptotic limit of 0.2 suggested in the *Gryning and Batchvarova (1994)* parameterisation probable is too high.
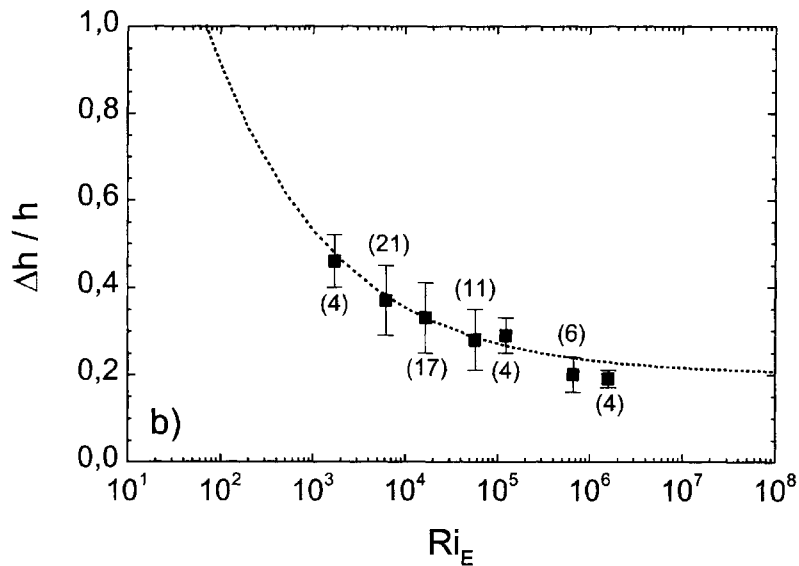
Figure 3.11. The normalised entrainment zone depth estimated from Sodar measurements and plotted against the entrainment Ri_E number, Eq. (2.12). The dashed line represent the parameterisation suggested by Gryning and Batchvarova (1994). The single data on the entrainment zone are grouped according to their Ri_E values. The figures indicate the number of cases in each class, and the error bars the standard deviation.

Comparison with a number of other parameterisations was in general not very successful although some dependence on dh/dt was found.

3.4 Validation summary

The simple applied model for the growth of the mixing height over homogeneous terrain was evaluated on our own measurements and also independently by a number of groups. The model was generally found to perform well. It was noted that the mechanical turbulence exerts a significant contribution to the growth of the mixing layer even at moderate wind velocities.

Simulations of the development of the internal boundary layer that forms downwind from a coastline 1) over land at onshore winds, and 2) over sea at offshore winds were carried out successfully. It is found that the quality of the model performance is associated with the possibility to include changes in wind direction and speed as well as the effect of the irregular coastline. In the independent model comparisons reported in Melas and Kambezidis (1992) and Källstrand and Smedman (1997) the simple slab model was found to perform best among a number (10 and 14) of expressions for the growth of the internal boundary layer. Källstrand and Smedman (1997) furthermore conclude that the model of *Gryning and Batchvarova (1990)* was the only one that agrees well with data from both small and larger distances from the coast.

The entrainment zone parametrization proposed by *Gryning and Batchvarova (1994)* was tested on a SANA data set by *Beyrich and Gryning, (1998)*. The relationship between $\Delta h/h$ and the entrainment Richardson number, Ri_E, in general was found to be good except in the limit of very large values of Ri_E where the measurements of $\Delta h/h$ turned out to be about 20% lower than predicted.

4 Boundary-layer height estimated from meteorological model output

Use of the simple applied model to calculate the height of the boundary layer requires *in situ* meteorological measurements, where the input to the model is either measured directly by *i. e.* a sonic anemometer, or can be derived by pre-processing of standard meteorological data such as wind speed, temperature and cloud cover.

When simulations with Numerical Weather Prediction (NWP) or meso-scale models are available it is common practice to estimate the height of the boundary layer from the model output, and the simple applied model is usually not used. However, the height of the boundary layer does not form a part of the output from the meteorological models, but has to be derived from the available output data.

Some of the advantages and shortcomings on the use of numerical meteorological models and the methods that are used to determine the height of the boundary layer will be considered. The discussion is based in part on a study of the formation of the marine boundary layer over the Baltic Sea and its predictability by a commonly used NWP-model (HIRLAM); and in part on simulations of the dynamics of the boundary layer during the PACIFIC-93 experimental campaign (see also chapter 3) in Vancouver, Canada, with the CSU-RAMS meso-scale model.

4.1 HIRLAM Model

The HIgh Resolution Limited Area Model HIRLAM is a complete model system for operational weather forecasts maintained by national meteorological services in Northern Europe. The baseline forecast model is a hydrostatic, semi-implicit limited area Eulerian

model described by Källén (1996). Operationally, local versions of the HIRLAM model are used, and in this study we use HIRLAM data provided by the Swedish Meteorological and Hydrological Institute. The horizontal grid resolution is 22.5 times 22.5 km and there are 31 vertical levels. Output from the simulations with the HIRLAM model includes hourly profiles of wind, temperature and humidity. Two methods to extract the boundary-layer height from the HIRLAM output data are applied and compared. Both are based on a bulk Richardson-number approach, but differ in the way the wind speed is taken into account. Starting from the lowest grid level the boundary-layer height is defined as the height, h, where the bulk Richardson number reaches a critical value.

Sørensen (1998) suggests the bulk Richardson number for the layer between the surface and the height z above the surface:

$$Ri_B = \frac{gz(\theta_v(z) - \theta_v(s))}{\theta_v(s)(u(z)^2 + v(z)^2)} \quad . \tag{4.1}$$

The quantities $\theta_v(s)$ and $\theta_v(z)$ are the virtual potential temperatures at the surface (by Sørensen (1998) taken as the lowest model level) and height z, respectively, $u(z)$ and $v(z)$ are the horizontal wind components (easterly and northerly usually) as function of height. Vogelezang and Holtslag (1996) suggest a Richardson-number where the wind is defined with respect to the lowest model level (here 30-m), and a term that accounts for surface friction has been added

$$Ri_B = \frac{gz(\theta_v(z) - \theta_v(s))}{\theta_v(s)[(u(z) - u(s))^2 + (v(z) - v(s))^2 + bu_*^2]} \tag{4.2}$$

where b is a parameterisation constant recommended to be 100. Sørensen (1998) and Vogelezang and Holtslag (1996) made an empirical estimate on the value of the critical Richardson number. Despite their differences in the formulation of the bulk Richardson numbers both studies found a value of 0.25 for the critical Richardson number to be adequate.

The expressions treat the wind-velocity influence differently. In Eq. (4.1) the wind speed is taken at the given height. Eq. (4.2) applies the difference between the lowest model level and the actual height, and the surface boundary layer is accounted for through an additional friction-velocity term which is not a part of the standard HIRLAM output but has to be parameterised. This term can be large compared to the wind-profile contribution. Then the boundary-layer height is determined mainly from the temperature profile and the friction velocity. Let us in crude terms consider the development of the atmospheric boundary layer over land (high surface roughness) and water (low surface roughness) for one and the same heat flux. The height of the boundary layer primarily is controlled by the heat flux (*Batchvarova and Gryning, 1991*). Over water owing to the small roughness length the wind speed is typically higher than over land and with smaller friction velocity. At a given height the Richardson number suggested by Sørensen (1998) would tend to be smaller over water than over land, and hence the critical Richardson over water should be smaller than the critical Richardson number over land. The effect of surface roughness on the critical Richardson number for the Vogelezang and Holtslag (1996) method is less evident, as this method operates on both the changes in the wind profile and the friction velocity.

The boundary-layer height deduced from HIRLAM output was compared to measurements of the marine atmospheric boundary layer that were carried out on Christiansø. The experimental campaign has already been described in Chapter 3.
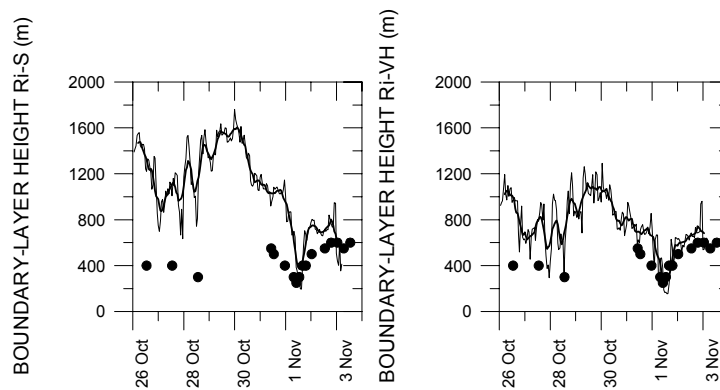

Figure 4.1. Boundary-layer heights over Christiansø during the extensive observation period, estimated from profiles of wind and temperature from the HIRLAM model, are shown by thin lines. The left panel shows the results using the Richardson number suggested by Sørensen (1998), the right panel when using the Richardson number in Vogelezang and Holtslag (1996). Bullets show the measurements. The thick line illustrates a running mean over 9 points.

The result from the analysis using the Richardson number suggested by Sørensen (1998) is shown in the left panel on Fig. 4.1. It can be seen that the predicted boundary-layer height is clearly too high during the first part of the experimental campaign where the wind is southwesterly. When the wind turns towards north such that Bornholm no longer affects the air mass over Christiansø, agreement between measurements and predicted boundary-layer heights improves considerably. The right panel shows the results when using the Richardson number suggested by Vogelezang and Holtslag (1996). It can be seen that the predicted boundary-layer height generally is substantially lower than on the left panel, but still overpredicts the boundary-layer height for the first part of the simulation where the wind passes over Bornholm before reaching Christiansø. The agreement is better during the last part when the wind is northerly and the effect of Bornholm is absent.

The poor result in combination with good results from the simulation with the simple slab model presented in chapter 3 suggests that the island of Bornholm controls the boundary layer over Christiansø during the first part of the period. The HIRLAM model grid is too coarse to resolve the effect of Bornholm.

During the last period of the experiment the wind was northerly. The air that reached Christiansø did not pass Bornholm on its way, but the water fetch to the nearest coast was about 100 km. For this case better agreement between measured and simulated boundary-layer heights was found for all the model simulations, indicating that for a water fetch of 100 km HIRLAM is able to resolve the change from land to sea.

The effect of the surface roughness on the critical Richardson number can be seen in the simulations of the boundary-layer height over Christiansø for long water fetches (westerly to northerly wind). *Gryning and Batchvarova (2003)* found the critical Richardson number that subjectively gave the overall best fit to the measurements to be 0.03 for the method suggested by Sørensen (1998) and 0.05 for Vogelezang and Holtslag (1996). This is illustrated in Fig. 4.2 where it also is evident that the Vogelezang and
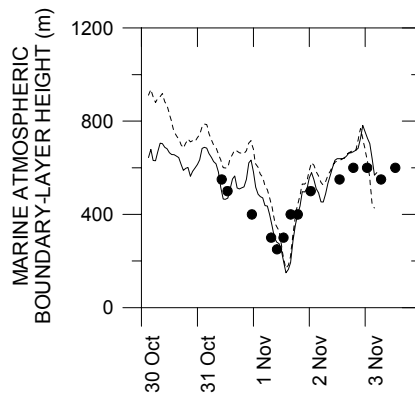
40

Figure 4.2. Height of the marine atmospheric boundary layer. The dashed line illustrates the boundary-layer height predicted by the method of Sørensen (1998) when applying a critical Richardson number of 0.03, the solid line shows the predictions of the Vogelezang and Holtslag (1996) with a critical Richardson number of 0.05. Bullets show measurements.

Holtslag (1996) method for this limited set of measurements gives a slightly better overall fit than Sørensen (1998).

4.2 The CSU-RAMS mesoscale model

The problem with the grid resolution in the NWP model can been overcome by use of a meso-scale model, but this solution is often not attractive because of the large computer resources required for the model runs. The Colorado State University Regional Atmospheric Modelling System (CSU-RAMS), described by Pielke *et al*. (1992) was applied for the PACIFIC-93 study (see chapter 3). The CSU-RAMS modelling system can be used under complicated meteorological and topographical conditions but it is a considerable effort to apply it for a given area. Xiaoming Cai, University of British Columbia, performed the simulations shown here with the CSU-RAMS modelling system. A grid size of 2.5 km times 2.5 km was used. Similar to a NWP models, the CSU-RAMS is not a model of internal boundary layer depth as such, but does give output from which the depth can be derived. In the present application, the top of the internal boundary layer is diagnosed from the vertical profile of TKE. The appropriateness of this is discussed in details in *Batchvarova et al. (1999)* from an examination of TKE profiles in the modelling area. By choosing a critical value of TKE, the top of the internal boundary layer can be identified. A typical value of maximum TKE in this area were about $0.5 \text{ m}^2\text{s}^{-2}$ and the critical value was chosen as $0.03 \text{ m}^2\text{s}^{-2}$. The internal boundary layer height was chosen as the first height from the ground at which TKE is smaller than the critical value.

Figure 4.3 shows the simulated and measured height of the internal boundary layer at Harris Road (see Fig. 3.4) 40 km downwind from the coastline. The agreement between measurements and model simulations is very good. It is interesting to note that the CSU-RAMS model is able to simulate the lowering of the mixed layer in the afternoon, and this is not the case for the simple slab model (Fig. 3.5). In chapter 3 it was noted that lowering of the mixed layer might be connected to local divergence in the wind field, a feature that the simple slab model cannot account for – the CSU-RAMS model seems to be able better to account for this phenomena.
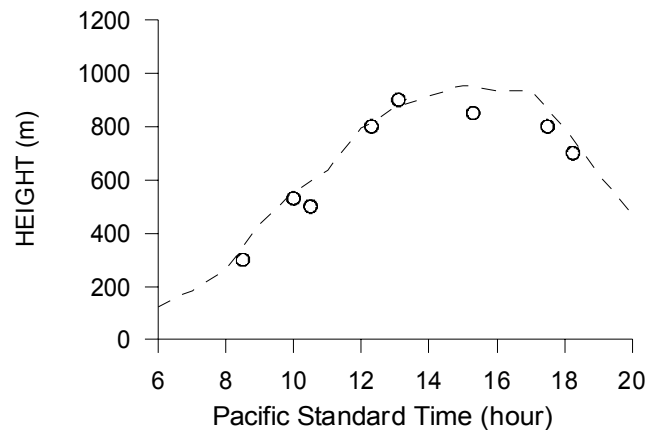
Figure 4.3. Temporal variation of the modelled internal boundary-layer height simulated with the CSU-RAMS model (dashed line), and the measured height at Harris Road.

Observed and modelled spatial structure of the internal boundary layer height along two (leg 1 and 3) of the three flight legs is shown in Figure 4.4 (see also Fig. 3.6).
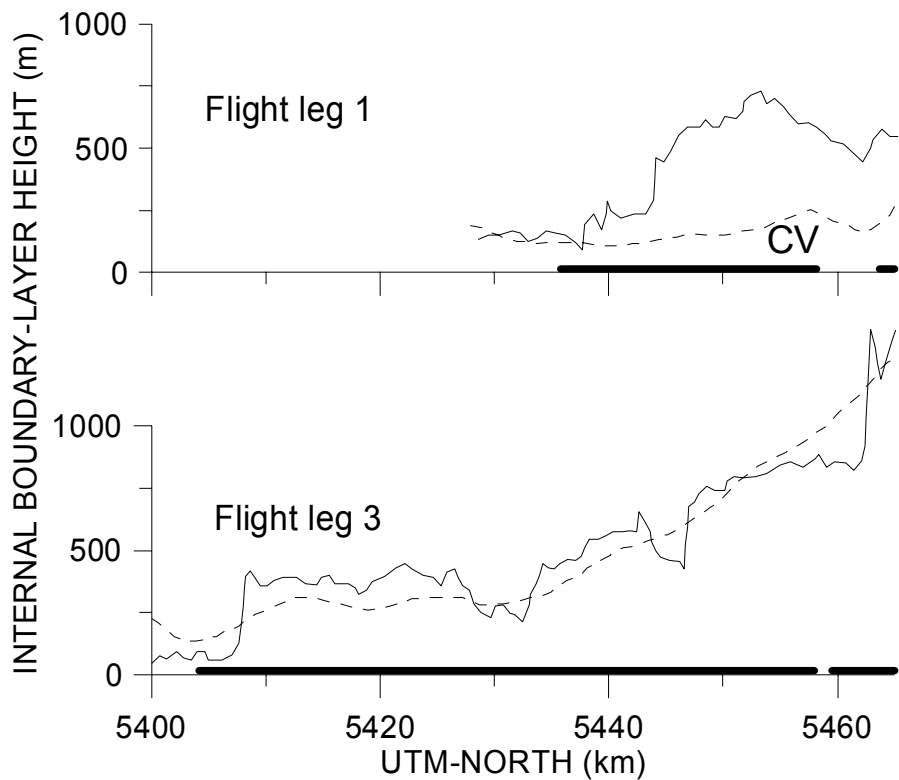
Figure 4.4. The spatial variation of the modelled internal boundary-layer height with the CSU-RAMS model (dashed line) and the measured height derived from aircraft data (solid line) along flight legs 1 and 3. The thick solid lines along the legs represent sections of land versus sea surface.

For the CSU-RAMS model the results badly underestimate the internal boundary layer in the city of Vancouver, flight leg 1. This is due to the fact that the model produces too strong a westerly sea breeze in this area, which decreases the overland fetch and consequently the internal boundary-layer height. It illustrates how sensitive the internal boundary layer height can be to a complex coastline where even small changes in the wind direction can result in pronounced variations of the overland fetch and

consequently have large effects on the internal boundary layer. Flight leg 3 captures more than 50 kilometres over land. The measurements and simulations agree very well along the flight leg.

Considering the complexity of the Lower Fraser Valley region the three-dimensional CSU-RAMS model performs reasonably well in this study, and particularly well in the central basin area. It is found that the success of this model relies on the correct reproduction of local wind field. This is generally a difficult task near the coast due to an inability to capture some sub-grid features and during the morning transition hours from land breeze to sea breeze.

4.3 Numerical meteorological models summary

The methods that are used to estimate the boundary layer height in numerical models depends on the model scale and output.

In operational meteorological forecast models output include profiles of wind, temperature and humidity, but usually not turbulence. For such models methods based on various formulations of bulk Richardson numbers are used to determine the height of the boundary layer.

Here we report findings from use of critical bulk Richardson numbers on HIRLAM model output in the marine environment. Two methods are applied. Generally the methods fail when the there is a major island upwind of the measuring site as is the case when Bornholm is about one grid length (~20 km) upwind of Christiansø. In this case the influence of Bornholm is hardly seen and the estimated boundary layer height over Christiansø is in not correct. When the upwind distance to the nearest coast is 4-5 grid lengths (~100 km) the ability to predict the marine boundary layer height with the Richardson number methods improves. The critical Richardson number can be argued to be a function of surface roughness, and best performance over water was found when using a critical Richardson number of around 0.05.

In the case that turbulence profiles are available from the model simulations, the bulk Richardson methods usually are not applied, but the boundary layer height is diagnosed from the vertical profile of turbulence. The case reported here - with the CSU-RAMS model - illustrate that the methods of a critical friction velocity generally performs well provided that the wind direction is correctly predicted. An example is given where the simulated wind direction in the coastal area gives a much shorter land fetch than in reality, thus the predicted boundary layer height is much lower than measured. Further inland, when the distance to the coast is less critical, the method works well.

5 Aggregation of fluxes over a patchy landscape

From the discussions in chapter 4 it is clear that the sub-grid variability of the mixed-layer height, momentum and sensible heat fluxes is believed to be an important but not yet settled issue for many model applications. Models for long-range transport and dispersion of atmospheric pollutants, Numerical Weather Prediction models, and Climate Models are all characterised by large grid cells that often enclose regions of pronounced inhomogeneities. The estimation of the regional or aggregated momentum and heat fluxes over non-homogeneous surfaces is therefore a central issue when the boundary conditions in models with large grid cells have to be specified.

Here is presented a method that can be used to determine the regional fluxes of momentum and sensible heat over chessboard type patchy landscapes (*Gryning and Batchvarova, 1999; Batchvarova et al., 2001*). The method is still in its infancy and under development. It is based on inverting the model for the prediction of the growth of the mixed layer - knowing the development of the mixed-layer height and with an estimate of the regional momentum flux, the aggregated heat flux of the upwind area can be estimated. It is applicable when the mixed-layer height is well above the layer where the individual surface heterogeneity is felt, for a detailed discussion see *Gryning and Batchvarova (1999)*. The required information for use of the method can be derived from wind speed and temperature profiles obtained by radiosoundings when they are performed frequently enough to provide a reasonably detailed structure of the mixed-layer development. Alternatively data from remote sensing techniques like combined wind profiler and radio acoustic sounding systems can be used.

5.1 Aggregation of momentum flux

The theoretical framework is the parameterized blending height method, in which the concept of momentum flux over an inhomogeneous area is as far as possible treated in analogy with the theories for homogeneous terrain, although the physics is far more complicated. When dealing with inhomogeneous conditions the regional (effective or aggregated) roughness length for momentum can be defined as the parameter that gives the correct surface stress for the area as a whole when used in connection with a wind profile relationship.
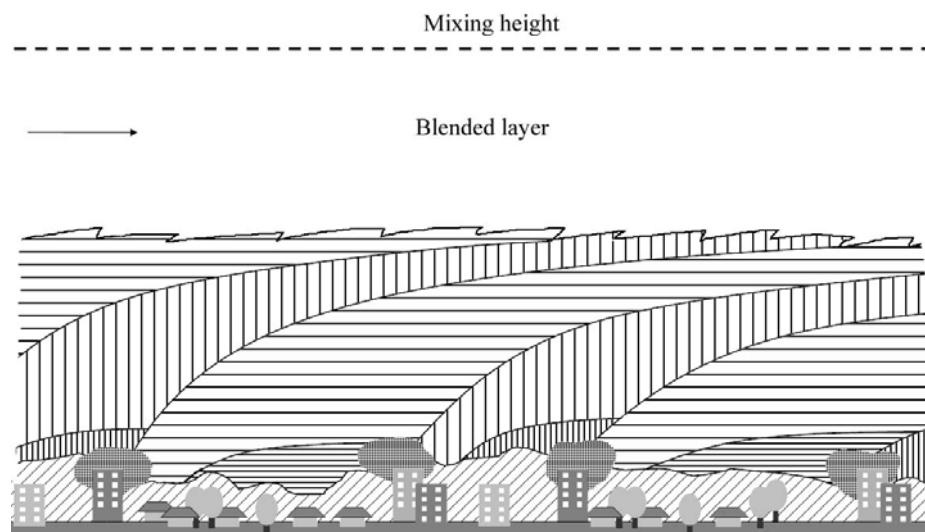

Figure 5.1. Schematics of the boundary layer structure over an urban area. The vertical and horizontal patterns represent the underlying surface of the neighbourhoods of tall and low buildings, respectively. Broad spaced patterns represent the urban internal boundary layers where advection processes are important. Fine spaced patterns show the inertial sublayers that are in equilibrium with the underlying surface and where Monin-Obukhov scaling applies. The forward slash pattern represents the roughness sublayer that is highly inhomogeneous both in its vertical and horizontal structure. The dotted pattern represents adjustment zones between neighbourhoods with large accelerations and shear in the flow near the top of the canopy. Above the height where the internal boundary layers are intermixed the effects of the individual neighbourhoods cannot be distinguished any more – the so-called blended layer.

The blending height, l_b, is the height where changes in surface conditions cannot be felt any more on the flow. It is illustrated for an urban area in Fig. 5.1. Mahrt (1996) gives as a rough estimate:

$$l_b = 2\left(\frac{\sigma_w}{u}\right)^2 L_c \tag{5.1}$$

where L_c is the typical length scale for the terrain inhomogeneities, σ_w and u are standard deviation of the vertical wind fluctuations and the wind speed at the blending height, respectively. Under neutral conditions the mean flow profile above the blending height becomes logarithmic with a roughness length corresponding the regional surface roughness and is independent of horizontal position. When the effect of stability is included into the wind profile it can be expressed as:

$$U(z) = \frac{u_*^{eff}}{\kappa} \left\{ \ln\left(\frac{z}{z_0^{eff}}\right) - \psi_m\left(\frac{z}{L^{eff}}\right) \right\} \qquad z > l_b \tag{5.2}$$

where κ is the von Karman constant, u_*^{eff} is the effective friction velocity, z_0^{eff} is the effective roughness length for the inhomogeneous area that will yield the correct surface stress from the wind profile and remains to be determined from the surface characteristics, ψ_m is the wind profile stability correction function and L^{eff} is the Monin-Obukhov length incorporating the effective momentum and sensible heat fluxes (Wood and Mason, 1991). Mason (1988) proposes that the drag coefficient at the blending height for the entire area should be estimated as the drag coefficients for the various sub areas weighted in proportion to their fraction of the area. For a homogeneous area the drag coefficient for near neutral conditions, C_{DN} is given by (Stull, 1988):

$$C_{DN} = \frac{\kappa^2}{\ln^2\left(z/z_0\right)} \qquad . \tag{5.3}$$

Therefore over a patchy landscape in neutral conditions:

$$\left[\ln\left(\frac{l_b}{z_0^{eff}}\right)\right]^{-2} = \sum_i f_i \left[\ln\left(\frac{l_b}{z_0^i}\right)\right]^{-2} \tag{5.4}$$

where f_i is the fraction of the total area covered by the ith surface having the local momentum roughness length z_0^i. The effective roughness length, z_0^{eff} represents the surface stress that originates from surface roughness and does not include the effect of major obstacles such as topography, houses and forest edges as discussed by Grant and Mason (1990). Wood and Mason (1991) found that while z_0^{eff} is a function of stability this dependence is small, and for all practical purposes can be neglected. The effective roughness length for the area can be determined by Eq. (5.4) from information on land-cover and blending height. In near-neutral conditions the stability dependence in Eq. (5.2) can be neglected. Knowing z_0^{eff} and l_b, the regional friction velocity, u_*^{eff}, at a given time can be determined from Eq. (5.2) by use of the wind-speed at the blending height that is known from i.e. radiosoundings.

5.2 Aggregation of sensible heat flux

The framework is the mixed-layer growth model by *Batchvarova and Gryning (1991) and (1994)*.

$$\left\{\frac{h^2}{(1+2A)h-2B\kappa L^{eff}}+\frac{C(u_*^{eff})^2 T}{\gamma g\left[(1+A)h-B\kappa L^{eff}\right]}\right\}\left(\frac{dh}{dt}-w_s\right)=\frac{\overline{(w'\theta')}_s^{eff}}{\gamma} \quad . \tag{5.5}$$

The potential temperature gradient, γ in the free atmosphere, the large scale vertical air velocity, w_s, the height of the boundary layer, h its growth rate, dh/dt and the rate of warming, $\partial\theta/\partial t$ of the free atmosphere above the mixing layer can be extracted from i.e. radiosoundings. The warming rate at height z in the free atmosphere is connected to the vertical velocity w_s and the potential temperature gradient at the same height through:

$$\frac{\partial\theta(z)}{\partial t}=-\gamma\, w_s(z) \quad . \tag{5.6}$$

For the special case when the horizontal divergence is constant with height the mean vertical velocity will be proportional to height

$$w_s(z)=-(div_H)z \tag{5.7}$$

where

$$(div_H)=\left(\frac{\partial\theta(z)}{\partial t}\right)z^{-1}\gamma^{-1} \quad . \tag{5.8}$$

At near neutral conditions when the stability correction in Eq. (5.4) can be omitted, u_*^{eff} can be determined independently of Eq. (5.5) which can be solved numerically for the vertical turbulent kinematic sensible heat flux at the surface, $\overline{(w'\theta')}_s^{eff}$, that is forcing the growth of the boundary layer. At unstable conditions Eqs. (5.2) and (5.5) become coupled and can be solved for u_*^{eff} and $\overline{(w'\theta')}_s^{eff}$ numerically by an iterative method.

5.3 An application

Use of the method is illustrated by an example(*Batchvarova et al., 2001*) taken from the WINTEX (Winter Experiment) campaign that was carried out during the period 12-24 March 1997 at the Finnish Arctic Research Centre near Sodankylä 100 km north of the polar circle in a sparse coniferous forest. The ground was covered with snow and the coniferous trees were snow-free most of the time. Days and nights were approximately equally long. Turbulence was measured by use of sonic anemometers above the forest (Gryning *et al.,* 2001). The Finnish Meteorological Institute released during the experiment radiosondes every three hours. On two occasions (15 and 17 March, 1997), a Lockheed C-130 aircraft operated by the UK Meteorological Office performed detailed measurements of meteorological variables over the area (Kangas *et al.*, 1998). The region is typical for the sub-arctic Northern Finland with coniferous and deciduous forests and large open mires dominating the landscape (*Batchvarova et al., 2001*). The region is rather flat both at small and large scales. The landscape is strongly heterogeneous in the sense that roughs forests (coniferous - 35%; deciduous and mixed

forest - 14%); smooth peat bogs and shrub lands (49%) and lakes and rivers (2%) are interspersed with a typical patch size of a few kilometres.

The regional momentum flux at the launch-time of each radiosoundings was determined from Eq. (5.2) using the regional roughness length and the wind speed at the blending height, which is available from the individual soundings. Fig. 5.2 illustrates the regional momentum fluxes as well as the local momentum fluxes above the forest on 15 March 1997.
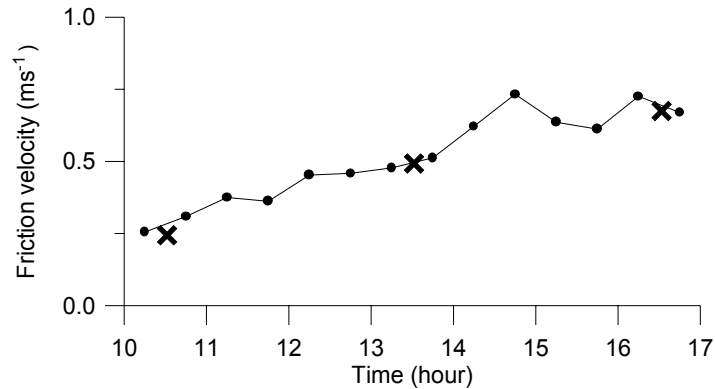

*Figure 5.2. Measured in situ local friction velocities over the forest at the Sodankylä Meteorological Observatory (18 metres above ground and 10 metres above the trees: •
connected by full line), derived regional friction velocities (×) from the blending height method based on radiosoundings launched from the Observatory for 15 March 1997. Time is given in LST.*

The regional momentum flux was found to be 10-20 % smaller than the local momentum flux over the forest. This shows that the forest roughness dominates the regional transport of momentum despite the fact that the forest occupies only 49% of the area. The open land is covered with snow and therefore rather smooth. Its contribution to the regional momentum flux is small.

Based on the radiosoundings, the evolution of the mixed layer, dh/dt, and its height, h, were determined by interpolation for every full hour. The gradient of the potential temperature, γ, in the free atmosphere was determined above the entrainment zone. The subsidence velocity was determined from the heating of the free atmosphere based on successive radiosonde temperature profiles. It turned out that large-scale subsidence was negligible. The regional sensible heat flux is illustrated in Fig. 5.3. It is found to be in fair agreement with the mean sensible heat flux along the flight-tracks of the research aircraft. For comparison the measured sensible heat flux over the forest is shown as well.

The regional sensible heat flux is significantly smaller than the sensible heat flux above the forest site. The surrounding area consists of mires and lakes, which were snow covered during the experiment and thus expected to have a relatively high albedo and consequently small sensible heat flux to the atmosphere. Further also the leafless deciduous forest is expected to contribute little to the sensible heat flux to the atmosphere. The area averaged sensible heat flux shows that the aggregated sensible heat fluxes are approximately 30-50% of the heat flux measured over the forest and agrees rather well with the land-use-weighted average sensible heat fluxes.
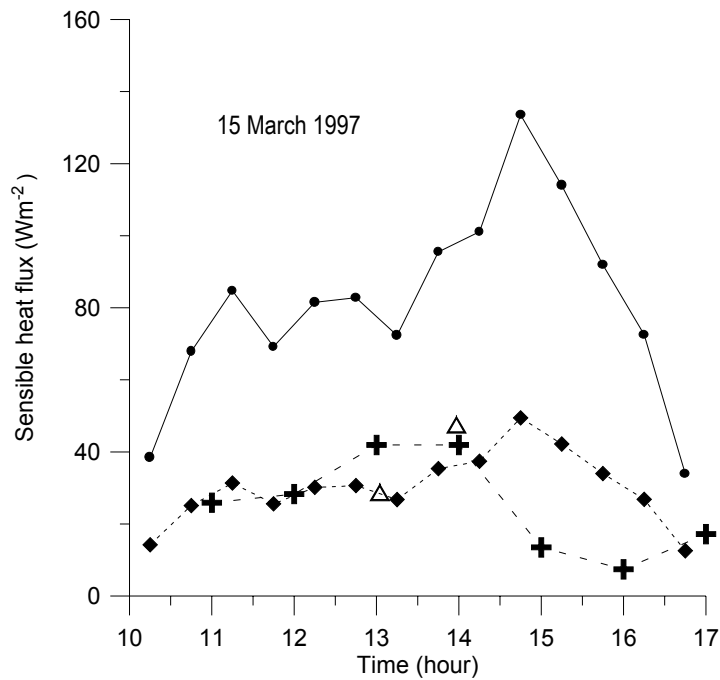
Figure 5.3. Measured local sensible heat flux over the forest at the Sodankylä Meteorological Observatory (18 metres above ground and 10 metres above the trees: • connected by a full line), the derived regional sensible heat flux (+ connected by a broken line), the flight-track mean values (Δ) and the land-use-weighted average heat fluxes (♦ connected by fine broken line) for 15 March 1997. Time is given in LST. The aircraft-measuring programme was performed in two 25-30 km long horizontal flights 50-100 m above ground level between 13 and 14 local time.

In summary, the forest dominates both the area averaged momentum and heat fluxes, but in quite different ways. The aggregated momentum flux is very close to the momentum flux over the forest, and only marginally dependent on the low roughness of the snow-covered areas. The aggregated sensible heat flux is considerable smaller than the heat fluxes over the forest and roughly the same as the land-use-weighted average sensible heat fluxes.

5.4 Aggregation summary

A new method to estimate aggregated momentum and sensible heat fluxes over a patchy landscape is presented. It is based on combining blending height theory and inverting the model for the growth of the mixing layer. An application for a sub-arctic landscape is presented.

6 Outlook

Most of the parameters that commonly are used to describe the turbulence in the atmospheric boundary layer represent conditions of atmospheric turbulence near the ground and have a small foot-print The mixing height is much more demanding in terms of requirements of homogeneous conditions because it overlooks a large area. Therefore, where it has been commonly accepted practice to use parameterisations for homogeneous terrain, even under inhomogeneous conditions, and the results have been good, this is not always the case for the mixing height.

From the discussions in the previous chapters it is clear that the size of the grid determines the features that the model can resolve, and therefore the scaling issue is essential for the prediction of the mixing height and boundary layer variables. The larger the grid the more of the small scale features in the flow field will not be resolved. Models for long-range transport and dispersion of atmospheric pollutants, Numerical Weather Prediction models, and Climate Models are all characterised by large grid cells. Sub-grid variability of the mixed-layer height and momentum and sensible heat fluxes is therefore an important but not yet settled issue for many model applications. A multitude of well established models have their roots in parameterisations of surface fluxes that have been developed for homogeneous terrain. The effect of their use in simple aggregation schemes over typical European areas that are characterised by a patchy structure of villages, towns, various types of agricultural fields and forests is not clear. Consequently the estimation of the regional or aggregated momentum and heat fluxes over non-homogeneous surfaces is a central issue when the boundary conditions in models with large grid cells have to be specified. In chapter 5 a new method is devised for the aggregation of momentum and heat fluxes over a patchy terrain. The required information for use of the method can be derived from wind speed and temperature profiles obtained by radio soundings when performed frequently enough to provide a reasonably detailed structure of the mixed-layer development. Alternatively data from remote sensing technique like combined wind profiler and radio acoustic sounding systems can be used.

The method was used during winter conditions over a sub-Arctic area with forest, fields, mires and lakes. The aggregated heat flux was found to be in general agreement with the land-use-weighted average heat flux (*Gryning and Batchvarova, 1999*; *Batchvarova et al., 2001*). Thus rough aggregation of the heat flux is simple, but *Batchvarova et al. (2001)* and Gryning and Batchvarova (2002a and 2002b) show that this is not the case for the momentum flux. For small patches Hasager and Jensen (1999) found that edge effects also have an effect on the aggregated heat fluxes. It is desirable to continue to investigate the blending of fluxes over patchy terrain, and extend the research to include aggregation for the urban area that today is virtually unknown. The urban area is far more complicated that the forest (Fig 5.1) and research in the formation of the local fluxes and the way they interact and finally forms the blending layer is very relevant for a better understanding of the urban climate.

Because the height of the boundary layer does not form part of the output from the models, it has to be estimated from the available output data. This is accomplished by use of methods based on either the turbulent kinetic energy or on various suggestions for the Richardson-number. But it is clear from this study, that this approach is still in its infancy and should be a topic for future research. First of all, advantages and disadvantages of the various Richardson numbers - the gradient Richardson-number, the bulk Richardson number, and the finite difference Richardson-number, are not clarified. Concerning the value of the critical bulk Richardson-number it is usually taken as 0.25, but *Gryning and Batchvarova (2003)* argues that over a smooth surface like the sea, the marine critical Richardson number can be expected to be smaller than over land. As a consequence of the large roughness over an urban area the urban critical Richardson number can be expected to be larger than 0.25. The urban boundary layer constitute a specific problem because it is horizontally inhomogeneous and characterised by greatly enhanced mixing from both the increased surface heating (natural and anthropogenic) and surface layer roughness. The urban area add an extra complication to the determination of the mixing height, because currently the urban effect in the NWP

models are included with great simplifications if included at all (Baklanov, 2002). The mixing height over the urban area is the topic for the COST715 in which context Baklanov (2002) concludes that the simple slab models such as *Gryning and Batchvarova (1996)* were found to perform well in the urban environment.

Therefore, the simple slab model is very well suited for simulations of the mixed-layer height, because it is computationally efficient, and because it can be operated on a very small grid size – say 500 metres. It is therefore able to simulate meso-scale features in the mixing height that models with a larger grid size cannot resolve. The NWP models are being operated on an increasing smaller grid, but even today it is far from the resolution that can be achieved with the simple slab model. However, it is my impression, that the wish to resolve the meso-scale features will continue the endeavour for a smaller grid, which together with the seemingly ever increasing computer resources eventually will reach the resolution of about one km which likely will fit with the resolution of the boundary conditions that it is realistically to achieve. It is my opinion, that the slab model despite the many simplifications is developed to such perfection that further refinements not likely will lead to substantial improvements. Future research on the mixing height and its spatial and temporal variability should be concentrated on NWP model output which, in principle, better can include more physical processes than a simple slab model. How to extract the boundary-layer height from the model output is still not clarified, and future research should be directed on the proper formulation of the Richardson-number and the parameters that are controlling its critical value.

Acknowledgements

List of symbols and acronyms

A : parameterisation constant

ABL : atmospheric boundary layer

ATHIBLEX : Athens internal boundary layer experiment

B : parameterisation constant

b : parameterisation constant

Bo : Bowen ratio

C : parameterisation constant

C^* : integration constant

C^{**} : integration constant

c_{DN} : drag coefficient for wind at neutral conditions

CBL : convective boundary layer

CSU-RAMS : Colorado State University regional atmospheric modeling system

CIRCE : Central Illinois rainfall chemistry experiment

COST715 : European cooperation in the field of scientific and technical research, #715

D : area

div_H : horizontal divergence

$\overline{e'}$: turbulent kinetic energy, TKE

$\overline{e'w'}$: vertical flux of turbulent kinetic energy

f_i : fraction of total area covered by the ith surface

g : acceleration due to gravity

g/T : buoyancy parameter

h : mixed layer height

h_0 : height to the lower part of the entrainment zone

h_2 : height to the upper part of the entrainment zone

h_{init} : initial height of the initial layer

HIRLAM : high resolution limited area model

LAT : local apparent time

LST : local standard time

L : Monin-Obukhov length

l_b : blending height

L_c : length scale for terrain inhomogeneity

L^{eff} : effective Monin-Obukhov length

MEDCAPHOT-trace : Mediterranean campaign of photochemical tracers – transport and chemical evolution

NOA : National observatory of Athens

NWP : Numerical weather prediction model

p : pressure

$\overline{p'w'}$: pressure velocity correlation

PEP : Pilot study on evaporation and precipitation over the Baltic Sea

PST : Pacific standard time

r : distance used in the interpolation procedure

RASS : radar acoustic sensing system

Ri_B : bulk Richardson number

Ri_E : entrainment Richardson number

s : surface or lower grid level

SANA : Study of the changing air pollution situation in eastern Germany after 1990

Sodar : sound detection and ranging

T : temperature

TKE : turbulent kinetic energy

u : wind velocity - alongwind or towards east

u_* : friction velocity

u_*^{eff} : effective friction velocity

UTC : coordinated universal time

UTM : universal transverse mercator

v : wind velocity – crosswind or towards north

WINTEX: Winter Experiment (Gryning et al. 2001).

w_s : mean vertical motion at the top of the mixed layer

x : downwind distance

z : height above ground

z_0 : roughness length

z_0^{eff} : effective roughness length

z_0^i : roughness length for the ith surface area (see also f_i)

γ : potential tempereture gradient above the mixed layer

δ : parameter in Eq. (2.14)

Δ : temperature jump at the top of the mixed layer

$(\Delta)_{GB}$: same as Δ

$(\Delta)_{\gamma=0}$:additional term that represent the effect of spin-up from w_*

Δh : entrainment zone thickness

ε : dissipation

η : parameter in Eq. (2.14)

θ : potential temperature

$\left(\overline{\theta'w'}\right)_h$: vertical kinematic heat flux at the top of the mixed layer

52

$\left(\overline{\theta'w'}\right)_s$: vertical kinematic heat flux at the surface

$\left(\overline{\theta_v'w'}\right)_s$: vertical virtual kinematic heat flux at the surface

$\left(\overline{\theta_v'w'}\right)_h$: vertical virtual kinematic heat flux at the top of the mixed layer

$\left(\overline{\theta'w'}\right)_s^{eff}$: effective vertical kinematic heat flux at the surface

κ : von Kármán constant

σ_w : standard deviation of the vertical wind fluctuations

ψ_m : wind profile stability correction

References

Argentini, S., Viola, A., Sempreviva, A. M. and Petenko, I. (2005) Summer PBL Height at the Plateau Site of Dome C, Antarctica. Submitted for publication in *Boundary-Layer Meteorol.*

Arya, S. P. S. and Byun, D. W. (1987). Rate Equations for the Planetary Boundary Layer Depth (Urban versus Rural*). Modelling the Urban Boundary Layer*. Amer. Meteorol. Soc., Boston, 215-251.

Baklanov, A. (2002). The Mixing Height in Urban Areas – a Review, *COST-Action 715 Workshop on Mixing height and inversions in urban area*, Toulouse 3-4 October 2001. EUR 20451. 9-28.

Batchvarova, E. and Gryning, S.E. (1991). Applied Model for the Growth of the Daytime Mixed Layer. *Boundary-Layer Meteorol.,* **56**, 261-274.

Batchvarova, E. and Gryning, S.E. (1994). An Applied Model for the Height of the Daytime Mixed Layer and the Entrainment Zone. *Boundary-Layer Meteorol.,* **71**, 311-323.

Batchvarova, E. and Gryning, S.E. (1998). Wind Climatology, Atmospheric Turbulence and Internal Boundary-Layer Development in Athens during the MEDCAPHOT-Trace Experiment. *Atmos. Environ.,* **32**, 2055-2069.

Batchvarova, E., Cai, X., Gryning, S.E. and Steyn, D. (1999). Modelling Internal Boundary-Layer Development in a Region with a Complex Coastline. *Boundary-Layer Meteorol.,* **90**, 1-20.

Batchvarova, E., Gryning, S.E. and Hasager, C. B (2001). Regional Fluxes of Momentum and Sensible Heat over a Sub-Arctic Landscape during late Winter. *Boundary-Layer Meteorol.,* **99**, 489-507.

Betts, A. K. (1992).'FIFE Atmospheric Boundary Layer Budget Methods. *J. Geophys. Res.,* **97**, 18523-18531.

Beyrich, F. (1995). Mixing Height Estimation in the Convective Boundary Layer using Sodar Data. *Boundary-Layer Meteorol.,* **74**, 1-18.

Beyrich, F. and Gryning, S.E. (1998). Estimation of the Entrainment Zone Depth in a shallow Convective Boundary Layer from Sodar Data. *J. Appl. Meteorol.,* **37**, 255-268.

Boers, R., Eloranta, E. W. and Coulter, R. L. (1984). Lidar observations of mixed layer dynamics: test and parameterized entrainment models of mixed layer growth. *J. Clim. Appl. Meteorol.,* **23**, 247-266.

Boers, R. and Eloranta, E. W. (1986). Lidar Measurements of the Atmospheric Entrainment Zone and the Potential Temperature Jump across the Top of the Mixed Layer. *Boundary-Layer Meteorol.,* **34**, 357-375.

Builtjes, P. J. H. (2001). Major Twentieth Century Milestones in Air Pollution Modelling and Its Application. *Air Pollution Modeling and Its Application XIV*, S.E. Gryning and F. Schiermeier (eds.), Kluwer Academic/Plenum Publishers, New York, 3-16.

Carson, D. J. (1973). The Development of a Dry Inversion-capped Convectively Unstable Layer. *Quart. J. Roy. Meterol. Soc.,* **99**, 450-467.

Cleugh, H. A. and Oke, T. R (1986). 'Suburban-rural Energy Balance Comparison in Summer for Vancouver. *Boundary-Layer Meteorol.,* **36**, 351-269.

Culf, A. (1992). An Application of Simple Models to Sahelian Convective Boundary Layer Growth. *Boundary-Layer Meteorol.,* **58**, 1-18.

Deardorff, J. W (1970). Convective Velocity and temperature Scales for Unstable Planetary Boundary Layer and Rayleight Convection. *J. Atmos. Sci.,* **27,** 1211-1213.

Deardorff, J. W. (1979). Prediction of Convective Mixed Layer Entrainment for Realistic Capping Inversion Structure. *J. Atmos. Sci.,* **36**, 424-485.

Deardorff, J. W., Willis, G. E. and Stockton, B. H (1980). Laboratory Studies of the Entrainment Zone of a Convectively Mixed Layer. *J. Fluid Mech.,* **100**, 41-64.

Driedonks, A. G. M. (1981). Dynamics of the Well-mixed Atmospheric Boundary Layer. *KNMI Sci. Rep. WR-81-2*, De Bilt. pp 189.

Driedonks, A. G. M. (1982). Models and Observations of the Growth of the Atmospheric Boundary layer. *Boundary-Layer Meteorol.*, **42**, 313-335.

Engelbart, D. (1997). Determination of mixed-layer depth using a 1290 MHz windprofiler/RASS. *COST-Action 76 Workshop on Profiler*, May 1997, Engelberg, Switzerland. Extensed abstracts edited by H. Richner, 286-289.

Gryning, S E. and Batchvarova, E. (2002a). Mixing Height in Urban Areas: Will 'Rural' Parameterisations Work. *COST-Action 715 Workshop on Urban Boundary layer Parameterisations.* EUR-20355, Zürich May 24-25 2001. 10 pp

Fay, B., Schrodin, R., Jacobsen, I., Engelbart, D. (1997). Validation of Mixing Heights Derived from the Operational NWP Models at the German Weather Service. *The Determination of the Mixing Height – Current Progress and Problems*. EURASAP Workshop Proceedings, 1-3 October 1997, Report Risø-R-997(EN), Risø National Laboratory, Roskilde, Denmark, 55-58.

Garratt, J. R. (1990). The Internal Boundary Layer. A Review. *Boundary-Layer Meteorol.,* **30**, 75-105.

Grant, A. L. M. and Mason, P. J (1990). Observations of Boundary-Layer Structure over Complex Terrain, *Quart. J. Roy. Meterol. Soc.,* **116,** 159-186.

Gryning, S.E., Ulden, A.P. van and Larsen, S.E (1983). Dispersion from a Continuous Ground-Level Source Investigated by a K-Model. *Quart. J. Roy. Meterol. Soc.,* **109**, 355-364.

Gryning, S. (1985). The Øresund Experiment - A Nordic Mesoscale Dispersion Experiment Over a Land-Water-Land Area. *Bull. Amer. Meteorol. Soc.,* **66**, 1403-1407.

Gryning, S.E., Holtslag, A.A.M., Irwin, J.S. and Sivertsen, B. (1987). Applied Dispersion Modelling Based on Meteorological Scaling Parameters. *Atmos. Environ.,* **21**, 79-89.

Gryning, S.E. and Batchvarova, E. (1990). Analytical Model for the Growth of Coastal Internal Boundary Layer during Onshore Flow. *Quart. J. Roy. Meterol. Soc.,* **116,** 187-203.

Gryning, S.E. and Batchvarova, E. (1994). Parametrization of the depth of the Entrainment Zone above the Daytime Mixed Layer. *Quart. J. Roy. Meteorol. Soc.,* **120,** 47-58.

Gryning, S.E. and Batchvarova, E (1996). A Model for the Height of the Internal Boundary Layer over an Area with a Irregular Coastline. *Boundary-Layer Meteorol.,* **78**, 405-413.

Gryning, S.E. and Batchvarova, E. (1999). Regional Heat Flux over the NOPEX Area Estimated from the Evolution of the Mixed Layer. *Agric. For. Meteorol.,* **98-99**, 159-168.

Gryning, S.E., Batchvarova, E. and De Bruin, H. A. R. (2001). Energy Balance of Sparse Coniferous High-Latitude Forest under Winter Conditions. *Boundary-Layer Meteorol.*, **99**, 465-488.

Gryning, S.E. and Batchvarova, E. (2002). Marine Boundary Layer and Turbulent Fluxes over the Baltic Sea: Measurements and Modelling. *Boundary-Layer Meteorol.,* **103**, 29-47.

Gryning, S E. and Batchvarova, E. (2002a). Mixing Height in Urban Areas: Will 'Rural' Parameterisations Work. *COST-Action 715 Workshop on Urban Boundary layer Parameterisations.* EUR-20355, Zürich May 24-25 2001. 10 pp

Gryning, S.E. and Batchvarova, E. (2002b). Regional Fluxes of Momentum and Sensible Heat over a Sub-arctic Landscape during late Winter. *Problems of atmospheric boundary-layer physics and air pollution. To the 80th birthday of professor M.E. Berlyand.* Chicherin, S.S. (ed.), Hydrometeoizdat, St. Petersburg, 202-215.

Gryning, S.E. and Batchvarova, E. (2003). Marine Atmospheric Boundary-layer Height Estimated from NWP Model Output. *Int. J. Environ. Pollut.,* **20**, 147-153.

Hasager, C.B., Jensen, N.O. (1999). Surface-flux Aggregation in Heterogeneous Terrain. *Quart. J. Roy. Meteorol. Soc.,* **125** , 2075-2102.

Holtslag, A. A. M. and van Ulden, A. P (1983). A Simple Scheme for Daytime Estimates of the Surface Fluxes from Routine Weather data. *J. Clim. Appl. Meteorol.,* **22**, 517-529.

Holtslag, A. A. M. and Nieuwstadt, F. T. M. (1986). Scaling the Atmospheric Boundary Layer. *Boundary-Layer Meteorol.,* **36**, 201-209.

Horst, T. W. (1979). Lagrangian Similarity Modeling of Vertical Diffusion from a Ground-level Source. *J. Appl. Meteorol.,* **18**, 733-740.

Højstrup, J.; Larsen, S.E.; Jensen, N.O. (1982). Results from an Experimental Investigation of a Step Change in Surface Heat Flux. *1. International Conference on Meteorology and Air/Sea Interaction of the Coastal Zone,* The Hague, 10-14 May 1982. American Meteorological Society, Boston, 28-30.

Kangas, M, Laine, V. and Heikinheimo, M. (1998). Use of C-130 Airborne Measurements in the Verification of Satellite Albedo Measurements in the Northern NOPEX/WINTEX Area. *Annales Geophysicae, Supplement IV to Volume 16*, p C1157.

Kerman, B. R., Mickle, R. E., Portelli, R. V., Trivett, N. B. and Misra, P. K. (1982). The Nanticoke Shoreline Diffusion Experiment - II. Internal Boundary Layer Structure, *Atmos. Environ.,* **16**, 423-437.

Klipp, C. and Mahrt, L. (2003). Conditional Analysis of an Internal Boundary Layer. *Boundary-Layer Meteorol.,* **108**, 1-17.

Klug, W. (1968). Diffusion in the Atmospheric Surface Layer: Comparison of Similarity Theory with Observations. *Quart. J. Roy. Meteorol. Soc.,* **94**, 555-562.

Källén, E. (1996). *Hirlam Documentation Manual, System 2.5*. SMHI, SE-601-76 Norrköping, Sweden. 180 pp.

Källstrand, B. and Smedman A.-S. (1997). A Case Study of the Near-Neutral Coastal Internal Boundary-Layer Growth: Aircraft Measurements Compared with Different Model Estimates. *Boundary-Layer Meteorol.,* **85**, 1-33.

Lilly, D. K. (1968). Models of Cloud-topped Mixed Layers under a Strong Inversion. *Quart. J. Roy. Meteorol. Soc.,* **94**, 292-309.

Luhar A.K (1998). An Analytical Slab Model for the Growth of the Coastal Thermal Internal Boundary Layer under Near-neutral Onshore Flow Conditions. *Boundary-Layer Meteorol.,* **88**, 103-120.

Mahrt, L. and Lenschow, D. H (1976). Growth Dynamics of the Convective Mixed Layer. *J. Atmos. Sci.,* **33**, 41-51.

Mahrt, L. (1979). Penetrative Convection at the Top of the Growing Boundary Layer. *Quart. J. Roy. Meteorol. Soc.,* **105,** 469-485.

Mahrt, L. (1996). The Bulk Aerodynamic Formulation over Heterogeneous Surfaces. *Boundary-Layer Meteorol.,* **78**, 87-119.

Manins, P. C (1982). The Daytime Planetary Boundary Layer: A New Interpretation of the Wangara Data. *Quart. J. Roy. Meteorol. Soc.,* **108**, 689-705.

Mason, P. J (1988). The Formation of Areally Averaged Roughness Lengths. *Quart. J. Roy. Meterol. Soc.,* **114,** 399-420.

Melas, D. and Kambezidis, H.D. (1992). The Depth of the Internal Boundary Layer over an Urban Area under Sea-Breeze Conditions. *Boundary-Layer Meteorol.,* **61**, 247-274.

Monin, A. S. and Obukhov, A. M. (1954). Basic Laws of Turbulence Mixing in the Ground Layer of the Atmosphere. *Akad. Nauk. SSSR, Geofiz. Inst. Trudy* **151**, 163-87.

Moussiopoulos, N. and Papagrigoriou, S.(editors) (1997). *Proceedings of the International Scientific Workshop "Athens 2004 Air Quality study".* Held 18-19 February 1997 in Athens, Greece. Available from the Athens 2004 Olympic Committee, Zappiro Megaro, Athens, Greece.

Nardino, M., Calzolari, F.,Georgiadis, T., Levizzani. V. and Sozzi, R (2001). Computing of the Mixed Layer Height through the Gryning-Batchvarova Model and Comparison with Experimental Data during MAP-SOP, MAP Newsletter (available from the MAP programme office, MeteoSwiss, CH-8044 Zürich, *15, 156-159.*

Nicholls, S. and Readings, C. S (1979). Aircraft Observations of the Structure of the lower Boundary Layer over the Sea. *Quart. J. Roy. Meteorol. Soc.,* **105**, 785-802.

Nyrén, K. and Gryning, S.E. (1999). Nomogram for the Height of the Daytime Mixed Layer. *Boundary-Layer Meteorol.,* **91** , 307-322

Obukhov, A. M. (1946). Turbulence in an Atmosphere with a Non-uniform Temperature. *Trudy Instituta Teoretichesko Geofiziki AN SSSR (Works of the Institute of Theoretical Geophysics, Acad. Sci. USSR, No 1).* Translated and published in *Boundary-Layer Meteorol.* **2**, 7-29.

Panofsky, H. A. and Dutton, J. (1984). *Atmopheric Turbulence.* John Wiley and Sons, pp 397.

Pasquill, F. (1974). *Atmospheric Diffusion (2en ed.).* Chichester, Ellis Horwood Ltd., pp 228.

Pielke, R., Cotton, W., Walko, R., Tremback, C., Lyons, W., Grasso, L., Nicholls, M., Moran, M., Wesley, D., Lee, T., and Copeland, J. (1992). A Comprehensive Meteorological Modelling System – RAMS., *Meteorology and Atmospheric Physics,* **49**, 69-91.

Portelli, R. V.(1982). The Nanticoke Shoreline Diffusion Experiment, June 1978-I. Experimental Design and Program Overview. *Atmos. Environ.,* **16** , 413-421.

Pottier, J., Thomson, B., Bottenheim, J., and Steyn, D. G. (1994). *Lower Fraser Valley Oxidants Study and Pacific'93 Meta Data Report.* Canadian Institute for Research in Atmospheric Chemistry. pp 50.

Raynor, K. N. and Watson, D. (1991). Operational Prediction of Daytime Mixed Layer Heights for Dispersion Modelling. *Atmos. Environ.,* **25A.** 1427-1436.

Schaller, E. and Seiler, W. (1993). Assessment of Photochemical Reactivity of the Atmosphere in former East Germany: the SANA-project. *Proc. 86th Ann. Meeting,* Denver, Colorado, Air Management Association, 1-10.

Seibert, P., Beyrich, F., Gryning, S.E., Joffre, S., Rasmussen, A. and Tercier, P. (1998). *Mixing height determination for dispersion modelling. Report of Working Group 2.* In: Harmonisation of the pre-processing of meteorological data for atmospheric dispersion models. COST action 710 - Final report. Fisher, B.E.A., Erbrink, J.J., Finardi, S., Jeannet, P., Joffre, S., Morselli, M.G., Pechinger, U., Seibert, P. and Thomson, D.J. (eds.). Office for Official Publications of the European Communities, Luxembourg, 1998, 120 p.

Seibert, P., Beyrich, F., Gryning, S.E., Joffre, S., Rasmussen, A. and Tercier, P. (2000). Review and Intercomparison of Operational Methods for the Determination of the Mixing Height. *Atmos. Environ.,* **34**, 1001-1027.

Soleiman, A. B. (2002). *Observations and Modelling of the near Equatorial Tropical Atmospheric Boundary Layer.* PhD-report. Institute of postgraduate studies and research. University of Malaya, Kuala Lumpur, Malaysia. 219 pp.

Stage, A. S. and Businger, J. A. (1981). A Model for Entrainment into a Cloud-topped Marine Boundary Layer, *J. Atmos. Sci.*, **30**, 1092-1099.

Steyn, D., and Oke, T. R. (1982). The Depth of the Daytime Mixed Layer at Two Coastal Sites: a Model and its Validation. *Boundary-Layer Meteorol.*, **24**, 161-180.

Steyn, D. (1990). An advective mixed layer model for heat and moisture incorporating an analytical expression for moisture entrainment. *Boundary-Layer Meteorol.*, **53**, 21-31.

Steyn, D., Bottenheim, J., and Thomson, R. (1997). Overview of Tropospheric Ozone in the Lower Fraser Valley, and the Pacific*'93 F*ield Study. *Atmos. Env.*, **31**, 2025-2035.

Stull R. B. (1976). The Energetics of Entrainment across a Density Interface. *J. Atmos. Sci*., **33**, 1260-1267.

Stull, R. B. (1988). *An Introduction to Boundary Layer Meteorology*, Kluwer Academic Publishers, Dordrecth, the Netherlands, pp 666.

Stunder, M. and SethuRaman, S (1985). A Comparative Evaluation of the Coastal Internal Boundary-layer Height. *Boundary-Layer Meteorol.*, **32**, 177-204.

Sørensen, J. H. (1998). Sensitivity of the DERMA Long-Range Gaussian Dispersion Model to Meteorological Input and Diffusion Parameters. *Atmos. Environ.,* **24**, 4195-4206.

Tennekes, H. (1973). A Slab Model for the Dynamics of the Inversion Above a Convective Boundary Layer. *J. Atmos. Sci.,* **30**, 558-567.

Tennekes, H. and Driedonks, A. G. M. (1981). Basic Entrainment Equations for the Atmospheric Boundary Layer. *Boundary-Layer Meteorol.,* **20**, 515-531.

Turner, D. B. (1970). *Workbook on Atmospheric Dispersion Estimates.* ,HPS Pub. 999-AP-26. pp 88.

Vogelezang, D. and Holtslag, A. (1996). Evaluation and Model Impacts of Alternative Boundary-Layer Height Formulations. *Boundary-Layer Meteorol.,* **81**, 245-269.

Wood N. and Mason, P. (1991). The Influence of Static Stability on the Effective Roughness Lengths for Momentum and Heat Transfer. *Quart. J. Roy. Meterol. Soc.,* **117**, 1025-1056.

Yordanov, D. and Batchvarova, E. (1988), Über die höhe der internen thermischen grenzschicht bei see-wind. *Z. Meteorol.,* **38**, 145-149.

Zeeman, O. and Tennekes, H. (1977). Parameterization of the Turbulent Energy Budget at the Top of the Daytime Boundary Layer. *J. Atmos. Sci*., **34**, 111-123.

Zilitinkevich, S. S. (1975). Comments on a Paper by H. Tennekes. *J. Atmos. Sci.,* **32**, 991-992.

Ziomas, I., Gryning, S.E. and Bornstein R.D. (Guest editors) (1998). The Mediterranean campaign of photochemical tracers - transport and chemical evolution (MEDCAPHOT-TRACE) Athens, Greece 1994-1995. Special issue in *Atmos. Environ.* **32**, 2043-2326.

Appendix. Budget of the turbulent kinetic energy

The slab model depicted in chapter 2 is developed by a combination of 3 equations from the heat conservation budget with a fourth that stems from the budget of the turbulent kinetic energy. The 3 equations from the heat budget are straightforward. The parameterisation of the turbulent kinetic energy budget is less trivial because it involves a number of assumptions and approximations (*Gryning and Batchvarova, 1994*).

In the convective mixed layer the turbulence is usually sufficient to maintain a uniform potential temperature from near the ground to its top, Fig. A.1. The so-called entrainment zone, a layer of strong stratification, caps the mixed layer.
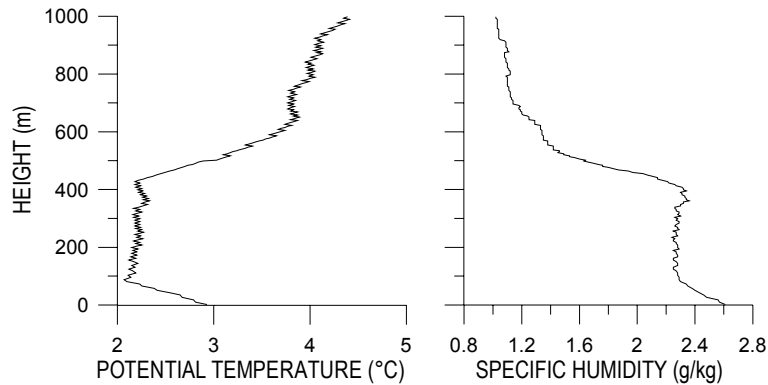
Figure A.1. Profile of potential temperature and humidity from a radiosounding carried out on a sunny day at Anholt on 29 March 1992 at 14:30. The mixed layer is the zone with near constant potential temperature (except very close to the ground) and humid air that extends from the ground to about 400 meters height. It is capped by the entrainment zone that extends from about 400 to 600 meters height, indicated by at sharp increase in the potential temperature and a drop of humidity. Above the entrainment zone in the free atmosphere the air is dry and stably stratified.
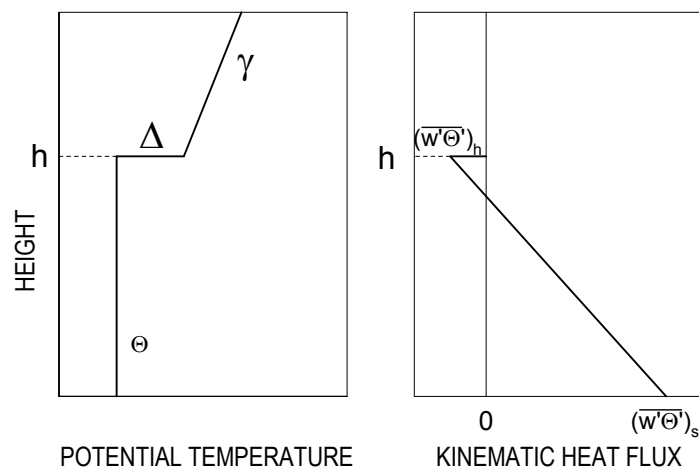
Figure A.2. Illustration of potential temperature and sensible heat flux profiles in the zero-order model of the mixed layer.

Fig. A.2 shows the idealised model adopted here, a so-called zero-order model. Inside the mixed layer the turbulence is assumed to be sufficient to maintain a uniform potential temperature with height and the entrainment zone is represented by an infinitesimally thin inversion. The air above the mixed layer is stably stratified. The model assumes

horizontal homogeneity. It can be seen from Fig. A.1 that the assumption of uniform potential temperature in the mixed layer is in accordance with measurements, whereas the representation of the entrainment zone is highly idealised.

The equation for the mean turbulent kinetic energy (TKE) under horizontal homogeneous conditions inside the mixed layer is (Stull, 1988):

$$\frac{\partial \overline{e'}}{\partial t} = \frac{g}{T}\overline{\theta'w'} - \overline{u'w'}\frac{\partial \overline{u}}{\partial z} - \frac{1}{\rho}\frac{\partial(\overline{p'w'})}{\partial z} - \frac{\partial(\overline{e'w'})}{\partial z} - \varepsilon \tag{A.1}$$

where $\overline{e'}$ is the turbulent kinetic energy, $\overline{\theta'w'}$ kinematic heat flux, $\overline{u'w'}$ momentum flux, $\overline{p'w'}$ is a pressure-velocity correlation, $\overline{e'w'}$ vertical flux of turbulent kinetic energy, ε is viscous dissipation, θ temperature and g acceleration due to gravity. Overbars indicate mean values, primes denote perturbation components. The turbulent kinetic energy equation can be integrated across the boundary layer to yield:

$$\int_0^h \frac{\partial}{\partial t}\overline{e'}dz = \int_0^h \frac{g}{T}(\overline{\theta'w'})dz - \int_0^h (\overline{u'w'})\frac{\partial \overline{u}}{\partial z}dz +$$
$$\left\{-(\overline{p'w'}/\rho)_h + (\overline{p'w'}/\rho)_s\right\} + \left\{-(\overline{e'w'})_h + (\overline{e'w'})_s\right\} - \int_0^h \varepsilon dz \tag{A.2}$$

where $(g/T)(\overline{\theta'w'})$ represents the buoyancy production and $(\overline{u'w'})\partial \overline{u}/\partial z$ the shear production of turbulent kinetic energy. The left-hand side of Eq. (A.2) can be written

$$\int_0^h \frac{\partial}{\partial t}\overline{e'}dz = \frac{\partial}{\partial t}\int_0^h \overline{e'}dz + \overline{e_h'}w_e \tag{A.3}$$

where w_e is the rate at which the mixed layer entrains into the top of the mixed layer and $\overline{e_h'}$ the turbulent kinetic energy at the top of the mixed layer. Mahrt and Lenschow (1976) considers the first term on the right-hand side of Eq. (A.3) small, arguing that the non-stationarity of the turbulent kinetic energy is significant only in the entrainment zone, represented by the second term. In the entrainment zone the turbulence is spin-up from its small value in the free atmosphere to the quasi-equilibrium state of the mixed layer (Zilitinkevich, 1975).

The first term on the right hand side of Eq. (A.2) represent buoyancy production of turbulent kinetic energy. As illustrated in Fig. A.2, it is negative near the entrainment zone and positive near the ground. An open question is how to partition the buoyancy-flux profile into production and consumption components. Here we use the so-called process-partitioning approach (Stage and Businger, 1981) in which the total buoyancy profile is split into a positive (producing) and negative (consuming) part. By assuming that both heat flux components vary linearly through the mixed layer, this term can be integrated to yield:

$$\int_0^h \frac{g}{T}(\overline{\theta'w'})dz = \frac{g}{2T}(\overline{\theta'w'})_s h + \frac{g}{2T}(\overline{\theta'w'})_h h \tag{A.4}$$

where the terms containing $(\overline{\theta' w'})_s$ indicates the production due to buoyancy of turbulent kinetic energy within the mixed layer and $(\overline{\theta' w'})_h$ reflects the consumption of kinetic energy associated with entrainment.

The second term is the mechanical production of turbulent kinetic energy. By introducing the thickness δ to account for jump conditions in the wind across the inversion it can be written:

$$\int_0^h (\overline{u' w'}) \frac{\partial u}{\partial z} dz = \int_0^{h-\delta} (\overline{u' w'}) \frac{\partial u}{\partial z} dz + \int_{h-\delta}^h (\overline{u' w'}) \frac{\partial u}{\partial z} dz \qquad (A.5)$$

where the first term represent the mechanical production of turbulent kinetic energy within the mixed layer and the second term the mechanical production of turbulent kinetic energy caused by the jump in wind-velocity across the inversion. The first term is important. The second term is generally considered small (Mahrt and Lenschow, 1976) but sometimes taken into account (Manins, 1982).

The third term on the right-hand side of Eq. (A.2) represents a loss associated with the radiation of internal gravity waves from the top of the entrainment zone to the free atmosphere. Stull (1976) found it to be negligible in most situations.

The fourth term in Eq. (A.2) represent the vertical flux of turbulent kinetic energy. Assuming that there is negligible turbulence in the free atmosphere this term become zero since it involves integration over h. The term neither creates nor destroys turbulent kinetic energy, but rather redistributes it within the mixed layer.

The considerations on the importance of the terms in the TKE budget is in agreement with experimental findings by Klipp and Mahrt (2003), who estimated the terms based on measurements drawn from the DUDAMEX experiment (Højstrup *et al.,* 1982). The data represent the development of a convective internal boundary layer over a beach and not a homogeneous mixed layer as discussed here. However, as illustrated in Fig. A.3, the buoyant and mechanical production and dissipation dominate the turbulent kinetic energy, in agreement with the above findings. (The advection term, shown in parenthesis on Fig. A.3, does not appear in the TKE equation for homogeneous conditions, but is characteristic for the internal boundary layer where it amounts to about 20% of the dominating terms).
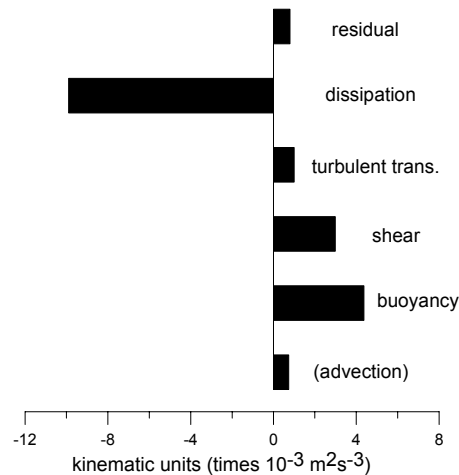

Figure A.3. The TKE budget terms inside a convective internal boundary layer (Klipp and Mahrt, 2003).

Omitting terms that are considered small the vertical mixed layer integrated turbulent kinetic energy budget can be written:

$$\overline{e'w}_e = \frac{g}{2T}(\overline{\theta'w'})_s h + \frac{g}{2T}(\overline{\theta'w'})_h h - \int_0^h (\overline{u'w'})\frac{\partial u}{\partial z}dz - \int_0^h \varepsilon dz \quad . \tag{A.6}$$

In parameterised form this can be expressed as

$$C\overline{e'w}_e = \frac{g}{T}(\overline{\theta'w'})_h h + A\frac{g}{T}(\overline{\theta'w'})_s h + Bu_*^3 \tag{A.7}$$

where A, B and C are dimensionless parameterisation constants. As we assume that dissipation is proportional to the turbulent kinetic energy production, the dissipation term is absorbed by the parameterisation constants.

Expressing the turbulent kinetic energy as function of u_* and rearranging we have

$$-\frac{g}{T}(\overline{\theta'w'})_h h + Cu_* w_e = A\frac{g}{T}(\overline{\theta'w'})_s h + Bu_*^3 \tag{A.8}$$

where the left hand side represent consumption of potential and kinetic energy by the entrainment process and the right hand side the main production terms of turbulent kinetic energy within the boundary layer. Solving for the downward directed heat flux at the inversion it reads:

$$-(\overline{\theta'w'})_h = A(\overline{\theta'w'})_s + \frac{Bu_*^3}{(g/T)h} - \frac{Cu_*^2}{(g/T)h}w_e \tag{A.9}$$

Often the spin-up term is omitted, in which case it simplifies to read:

$$-(\overline{\theta'w'})_h + = A(\overline{\theta'w'})_s + \frac{Bu_*^3}{(g/T)h} \tag{A.10}$$

The usual value of A is 0.2 (Tennekes, 1973; Stull, 1976) but recent experimental results from different climatic regions suggest a higher value of around 0.4 (Betts, 1992; Culf, 1992). For B Tennekes (1973) proposes 2.5 and Driedonks (1981;1982) obtained best results with 5. Based on Zilitinkevich (1975) and Tennekes and Driedonks (1981) the value of C can be estimated to around 8. Beyrich (1995) propose to adapt the model constants to actual observation from e. g. Sodar or wind profiler data for the specific area and conditions in order to improve the model results.

The air has been assumed dry and the effect of water vapour is unaccounted for. Because water vapour has a lower density than dry air it decreases the density of the air. The combined effect of temperature, T, and specific humidity q may be represented by the virtual temperature $\theta_v = \theta(1 + 0.61 q)$ and the combined heat flux, accounting for both latent and sensible heat fluxes, becomes

$$\overline{\theta_v'w'} = \overline{\theta'w'} + 0.61T\overline{q'w'} \tag{A.11}$$

which by introducing the ratio of the sensible to latent heat fluxes, $Bo = \gamma_p \overline{\theta'w'}/\overline{q'w'}$ where γ_p is the psychrometric constant, can be written as

$$\overline{\theta'_v w'} = \overline{\theta' w'}\left(1 + 0.07/Bo\right) \tag{A.12}$$

where Bo is the Bowen ratio (Stull, 1988). It can be seen that the inclusion of water vapour increases the kinematic heat flux in Eq. (A.1) but the effect is small. In a study of the tropical boundary layer Soleiman (2002) found the effect on the mixing height of the tropical boundary layer to be less than 10%.

Mission

To promote an innovative and environmentally sustainable technological development within the areas of energy, industrial technology and bioproduction through research, innovation and advisory services.

Vision

Risø's research **shall extend the boundaries** for the understanding of nature's processes and interactions right down to the molecular nanoscale.

The results obtained shall **set new trends** for the development of sustainable technologies within the fields of energy, industrial technology and biotechnology.

The efforts made **shall benefit** Danish society and lead to the development of new multi-billion industries.